UNIVERSITY OF CALIFORNIA SAN DIEGO

# Investigation of a Human Monomeric NEET Protein MiNT:

# Structural Properties and Comparison to Homologous Human NEET Proteins, mNT and NAF-1

A thesis submitted in partial satisfaction of the requirements for the degree Master of Science

in

Chemistry

by

Christopher Susanto

Committee in charge:

Professor Patricia A. Jennings, Chair
Professor Michael J. Tauber
Professor Emmanuel A. Theodorakis

2019

The Thesis of Christopher Susanto is approved, and it is acceptable in quality and form for publication on microfilm and electronically:

---

---

---

Chair

University of California San Diego

2019

EPIGRAPH

*“Iron Sharpens Iron, as one man sharpens another”*

**Proverbs 27:17 (ESV)**

Table of Contents

Signature page ……..……iii

Epigraph …….....iv

Table of Contents ……v

List of Abbreviations …….....vi

List of Figures …….……viii

List of Tables…….……...x

Acknowledgements…….……xi

Abstract of the Thesis……xiii

Chapter 1 General Introduction……..1
1.1 Iron sulfur proteins and cluster biogenesis…….…….....2
1.2 Introduction to NEET proteins……...3
1.3 Third member of human NEET protein MiNT……..4
1.4 Present analysis on MiNT……...7

Chapter 2 General Methods……8
2.1 Introduction…...……..…….……9
2.2 Methods……..……..11
2.2.1 Transformation Protocol……..……...11
2.2.2 Construction and verification of plasmids……..11
2.2.3 Expression checks and glycerol stocks……...14
2.2.4 SDS-PAGE…...……..……15
2.2.5 Growth of cells and purification of proteins…….…..16

2.3 Biophysical assays and analysis…….…..19

Chapter 3 MiNT: Effects of a C-terminal Histidine Tag and Purification Efficiency of WT and Mutants…….....20
3.1 Introduction……..21
3.2 Results and discussion……..……21

Chapter 4 Characterization of human monomer NEET protein MiNT: Inheritance of both clusters in a single polypeptide and consequence on its properties……35
4.1 Introduction…..……..……...…36
4.2 Results and discussion…….37

References……..51

List of Abbreviations

| | |
|---|---|
| BME | *β*-mercaptoethanol |
| cam | chloramphenicol |
| CBD | cluster binding domain |
| CIA | cluster iron sulfur cluster assembly |
| CD | circular dichroism |
| CISD | CDGSH iron Sulfur Domain |
| COPD | chronic obstructive pulmonary disease |
| C-terminal | carboxyl terminal |
| DH5α | DH5-alpha cells |
| DM | double mutant |
| DNA | deoxyribonucleic acid |
| DNAse I | deoxyribonuclease I |
| DTT | dithiothreitol |
| *E. Coli* | *Escherichia coli* |
| EPR | electron paramagnetic resonance |
| ER | endoplasmic reticulum |
| FDX | ferredoxin |
| FPLC | fast protein liquid chromatography |
| His-tag | histidine tag |
| IEX | ion exchange |
| IMAC | immobilized metal affinity chromatography |
| IPTG | isopropyl β-D-1-thiogalactopyranoside |
| ISC | iron sulfur cluster |
| kan | kanamycin |
| kDa | kilodalton |
| LB | Luria-Bertani |
| LC-MS | liquid chromatography mass spectrometry |
| MAM | mitochondrial associated membrane |
| MI | myocardial infarction |

| | |
|---|---|
| MiNT | mitochondrial inner NEET protein |
| mNT | mitoNEET |
| NAF-1 | nutrient-deprivation autophagy factor 1 |
| N-terminal | amino terminal |
| NIF | nitrogen fixation |
| OD | optical density |
| PCR | polymerase chain reaction |
| PFV | protein film voltammetry |
| pI | isoelectric point |
| PMSF | phenylmethylsulfonyl fluoride |
| PPARγ | peroxisome proliferator-activated receptor γ |
| ROS | reactive oxygen species |
| SDS-PAGE | sodium dodecyl sulfate- polyacrylamide gel electrophoresis |
| S.O.C | super optimal broth with catabolite expression |
| SUF | sulfur assimilation |
| TZD | thiazolidinedione drug |
| UV-Vis | ultra violet – visible light |
| WT | wild type |

List of Figures


Figure 1.1: Structure of common iron-sulfur clusters…….……2

Figure 1.2: General amino acid sequence alignment of three human NEET protein…..…….5

Figure 1.3: Crystal structure of the human NEET protein……..5

Figure 2.1: Sequence of WT MiNT……..12

Figure 3.1: Protein expression for tagged MiNT constructs…….....22

Figure 3.2: 15% SDS-PAGE gel of WT-tag construct using IMAC purification……..…23

Figure 3.3: Crystal structure of DM MiNT……...24

Figure 3.4: Cation exchange purification step for the DM-tagged MiNT construct using a gradient elution from 30 mM to 600 mM NaCl…….....25

Figure 3.5: SDS-PAGE of DM-tag construct for all purification steps from IMAC to IEX…….....26

Figure 3.6: FPLC chromatogram of non-tagged DM construct during subsequent IEXs…….27

Figure 3.7: Third cation exchange elution fraction of all four, separate non-tagged MiNT constructs……...28

Figure 3.8: Chromatogram of S200 size exclusion column purification step for WT and DM constructs……...29

Figure 3.9.1: Liquid chromatogram in LC-MS using ESI-TOFMS for the purified sample from the S200 non-tagged WT elution……...30

Figure 3.9.2: Liquid chromatogram in LC-MS using ESI-TOFMS for the purified sample from the S200 elute non-tagged DM construct elution……..30

Figure 3.10: 15% SDS-PAGE ending with S200 column purification for non-tagged constructs……...31

Figure 3.11: Size exclusion chromatogram of all non-tagged MiNT constructs with a S100 size exclusion column……...32

Figure 3.12: 15% SDS-PAGE gel for all non-tagged constructs after full purification…….....33

Figure 3.13: Liquid chromatogram in LC-MS using ESI-TOFMS for the purified sample from S100 WT elution……34

Figure 4.1: Stability of the iron-sulfur clusters for all constructs of MiNT with time at 25 °C using 458 nm peak for each scan……...37

Figure 4.2: Stability of the iron-sulfur clusters for all constructs of MiNT with time at 37 °C using 458 nm peak for each scan……...38

Figure 4.3: Absorption scan between 250 to 800 nm wavelength of MiNT and its mutants……...38

Figure 4.4: Circular dichroism spectra of MiNT and its mutants scanned in a range of 200 nm to 300 nm at 15 °C…….…….39

Figure 4.5: Circular dichroism spectra of MiNT and its mutants scanned in a range of 300 nm to 800 nm at 15 °C…….…….42

Figure 4.6: Comparison spectra between UV-Vis and circular dichroism assay for all MiNT constructs…….....43

Figure 4.7.1: DM UV-Vis spectra of 30 μM protein sample with 15 mM DTT at 15 °C in 50 mM Tris pH 8.0 and 150 mM NaCl buffer …….....45

Figure 4.7.2: H75C UV-Vis spectra of 30 μM protein sample with 15 mM DTT at 15 °C in 50 mM Tris pH 8.0 and 150 mM NaCl buffer ……...45

Figure 4.7.3: H113C UV-Vis spectra of 30 μM protein sample with 15 mM DTT at 15 °C in 50 mM Tris pH 8.0 and 150 mM NaCl buffer ……...46

Figure 4.7.4: WT UV-Vis spectra of 30 μM protein sample with 15 mM DTT at 15 °C in 50 mM Tris pH 8.0 and 150 mM NaCl buffer …….....46

Figure 4.8: Crystal structure of DM MiNT construct continued……..48

List of Tables

Table 2.1: Amino acid sequence of MiNT (36-127) with highlighted single point mutations for each construct……...10

Table 2.2: Designed primers for deletion and substitution mutations…….…....13

Table 2.3: Recipe for PCR sample reactions with various amounts of double stranded DNA……...13

Table 2.4: Program used for thermal cycler……14

Table 2.5: List of reactants and volumes to make 15% acrylamide SDS-PAGE gel……..15

Table 3.1: Constructs of MiNT showing the molecular weight without 2Fe-2S clusters and the isoelectric point……..21

Table 3.2: Concentration of buffer and salts that are used for IMAC…….…….....23

ACKNOWLEDGEMENTS

This work would not have been possible without everyone involved in my whole curriculum and experience in UCSD. Firstly, I would like to thank Professor Patricia A. Jennings for giving me this opportunity for a wonderful project in NEET proteins. It is extremely difficult to find a correct fit into a laboratory especially as a Masters student with limited time for research, not to mention as an international student planning to go into a thesis track. I am very grateful for Professor Theodorakis for guiding me to the right settings as a new student, especially also being very knowledgeable in my current project. I would also like to thank Professor Tauber taking the time to teach me on using circular dichroism techniques and troubleshooting.

In my experience working in this laboratory, I realized that how crucial every member of the lab have to work as a body towards the common goal in research. Together, it creates a healthy culture of a workplace that I could never hope to expect. I would like to thank Jason, a fellow graduate student of the similar project, for the patience on training me and answered my questions as best as possible, when I was inheriting the project from another graduate student Colin. I am also very grateful of the purchases that he made for me that is needed for the experiments and taught me to time my experiments efficiently even if it required to start at 4 am. Professor Jennings, Kendra and Dom have been extremely helpful in troubleshooting the problems using their vast experience in regards to troubleshooting problems and suggesting new experiments. All members of my laboratory have been very approachable and allow me to be very flexible with my schedule on both purification and assay experiments. I would also like to thank Nick for giving me a chance on his role to be an area safety coordinator to maintain the lab and train new students.

Professor Jennings has also helped me in many aspects in both knowledge and allowing me to experience constructive criticism in a class she taught that catered to all fields. That gave me a great experience on how realistic the world looks like when presenting a research from a biochemist perspective and to expect the unexpected. Classmates namely Aashish, Meihan, Douglas and James to name a few from

the same course also helped me overcome the passiveness in me by being supportive and using their respective field's experience to better improve the approach on research though they might not work on the same project as I am. This also created a small community in the UCSD chemistry graduate department and allows me to be ready anytime they are having any emergency.

Outside of the department, I would also like to thank my friends in San Diego Lighthouse Bible Church, Charles and Jeremy who keep me grounded on the principles in life and my conduct in check at all times. I would also like to thank my close friends situated in Los Angeles area namely Huy, Hung, Tri and Bill as they have been a huge support during undergraduate times till now even though they are extremely busy with their pharmacy curriculum. I would also not be able to complete the journey without my close friends back in Singapore mainly Oscar, JP and a few others on their support since middle school.

Lastly, I would like to thank my family for them believing in me through school all these years and beyond. Without their support, I would not be able to have the opportunity to study in the United States, having a much different experience than back home. I cannot express eternal gratitude for that other than showing them the fruits of their labor for their time and effort in me.

ABSTRACT OF THE THESIS

Investigation of a Human Monomeric NEET Protein MiNT:

Structural Properties and Comparison to Homologous Human NEET Protein, mNT and NAF-1

by

Christopher Susanto

Master of Science in Chemistry

University of California San Diego, 2019

Professor Patricia A. Jennings, Chair

Iron-sulfur cluster proteins are considered to be one of the most ubiquitous prosthetic groups since ancient times. Regulations of iron homeostasis through iron-sulfur proteins is of critical importance for cell development as free labile iron can cause DNA and lipid damage, lesions and ultimately cancer from production of reactive oxygen species (ROS). The unique NEET class of proteins harbors 3 Cys- 1 His ligand configuration having a consensus sequence of [C-X-C-X2-(S/T)-X3-P-X-C-D-G-(S/A/T)-H] that houses 2Fe-2S clusters. This thesis focuses on

a monomeric human NEET protein MiNT found within the mitochondrial matrix as opposed to the dimeric mNT and NAF-1. Though MiNT has an upregulated expression in cancer cells and 2Fe-2S cluster properties are similar to mNT and NAF-1, not much is known about it. Characterization of MiNT's structure function relationships are studied in subsequent chapters in order to understand the effects of its asymmetry by doing a point mutation on the histidine at position 75 and 113 individually and both. Ultra-violet visible spectroscopy (UV-Vis) and circular dichroism (CD) will be employed to further understand MiNT's unique differences as a monomeric protein carrying both clusters. These assays show that there are effects on the stability by temperature and structure differences are analyzed through the differences of the CD spectra. Comparison of spectra between oxidized and reduced state in UV-Vis for all constructs show that a possible tryptophan residue is responsible for acting as an electron transfer hub between the two clusters in MiNT, not noticed in the other human NEET proteins.

# Chapter 1

# General Introduction

## 1.1 Iron sulfur proteins and cluster biogenesis

Iron-sulfur clusters are considered one of the most abundant and adaptable prosthetic groups present in an enzyme or a protein. They are composed of non-heme iron and inorganic sulfide, and have existed since ancient times (1, 2). Iron has been essential as a cofactor for nitrogen fixation, photosynthesis and respiration on both prokaryotes and eukaryotes, and is one of the most abundant transition metals on earth (3). Due to its abundance, iron-sulfur clusters are considered to be one of the most primitive iron cofactors known in biology (4). Some of the common clusters that can be found in iron-sulfur proteins are [2Fe-2S], [3Fe-4S], and [4Fe-4S] having typical cysteine ligands as shown below in **Figure 1** (2, 5).

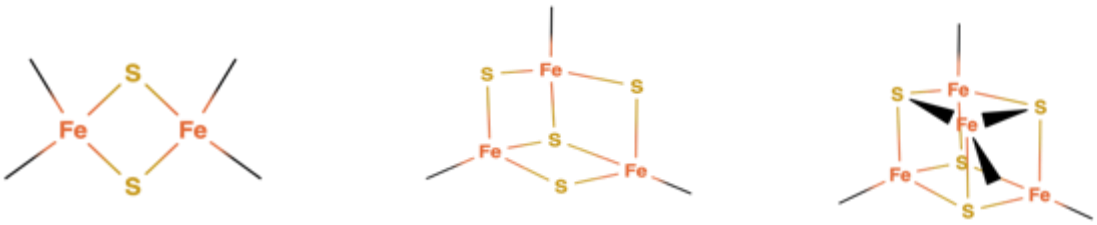


**Figure 1.1: Structure of common iron-sulfur clusters**. [2Fe-2S] having a rhombic assembly, [3Fe-4S] a half cubane and [4Fe-4S] cubane shaped.

As mentioned before, iron-sulfur proteins have a diverse range of functions in a cell. Of critical importance, iron-sulfur clusters can attain various redox states with a large range from +500 mV to less than -500 mV, promoting electron transfer catalysis (6). Iron-sulfur clusters are modular, resulting in interconversion between different iron-sulfur proteins due to its obtainable mixed valence states (7). As such, iron-sulfur proteins have exceptional spectroscopic and chemical properties for characterization (6-8). Iron-sulfur cluster proteins can also react as a biological sensor, typically with oxygen and nitric oxide to regulate cell development (9). In bacteria, three distinct pathways for iron-sulfur cluster biosynthesis are identified, mainly the iron-sulfur cluster (ISC) system pathway, nitrogen fixation (NIF) system

pathway, and sulfur assimilation (SUF) system pathway (10-12). Many organisms possess more than one, highly conserved, iron-sulfur cluster biosynthesis pathway due to critically important roles these clusters play in numerous pathways (13, 14). Human cells have two sets of iron-sulfur cluster production machinery, mainly the ISC export pathway present in the mitochondria for cluster maturation, to be used in the cytosolic iron-sulfur cluster assembly (CIA) pathway outside of the mitochondria (15, 16). Biosynthesis of iron sulfur proteins is believed to be initiated in the mitochondria in the ISC pathway and eventually exported out into the cytosol by the mitochondrial ABC transporter Atm1 (human ABCB7) (15).

## 1.2 Introduction to NEET proteins

Species- wide proteomic studies show that the amount of iron handling in eukaryotic cells is much greater than that of another transition metal, copper since copper handling only constitutes to 1% in both prokaryotic and eukaryotic cells in organ and metabolic processes (17, 18). In human cells, the majority of cellular iron can be found sequestered by proteins in the mitochondria and the cytosol, acting as a cofactor for DNA biosynthesis and repair, small molecule binding partners and preventing free/labile iron accumulation which can lead to dangerous levels of reactive oxygen species (ROS) generation through Fenton catalytic process (15, 19-20). Labile iron in human cells has detrimental effect as it has been known to be linked to cardiovascular and kidney diseases, neurodegenerative diseases such as Friedreich's ataxia, Parkinson's and Alzheimer's disease, and even cancer cell death (21-26). Fundamentally, [2Fe-2S] clusters are considered as the simplest cluster and are used as building blocks to create the more complex cubane shaped [4Fe-4S] cluster in the later stages of ISC or CIA pathway (17, 27). Common ligands to iron-sulfur clusters in proteins are cysteines (17). Example [2Fe-2S] cluster proteins are ferredoxins (FDX) having 4- Cys ligands and Rieske proteins having 2 Cys-2 His ligands (28-30). NEET proteins however, are an unusual class of proteins that harbor a 3

Cys- 1 His ligand configuration (31). NEET proteins belong to a unique CDGSH domain with a consensus sequence of [**C**-X-**C**-X2-(S/T)-X3-P-X-**C**-D-G-(S/A/T)-**H**].

The first outer mitochondrial membrane human NEET protein is coined mitoNEET or CDGSH iron-sulfur domain 1 (mNT, CISD1). It was originally identified as a target of a type II diabetic drug pioglitazone, a thiazolidinedione sensitizer and thus named NEET from its Ans-Glu-Glu-Thr (NEET) sequence protein (31). Using tritiated pioglitazone and photoaffinity cross linker, identification of mitoNEET as a target was found through binding studies (32). Thiazolidinedione drugs (TZDs) were initially thought of as only serving as a direct activating agent to a nuclear receptor peroxisome proliferator-activated receptor γ (PPARγ) but knockout studies suggest that there are other possible targets due to similar anti-inflammatory effects (33). Also, rosiglitazone, another TZD, which potentially increases chances of myocardial infarction (MI) and pioglitazone usage as a treatment in neurodegenerative diseases suggest that mNT is a potential target of the mentioned drugs (34-37). Stabilization of mNT in the presence of pioglitazone also suggests it is a feasible alternative target (31).

The second homolog human NEET protein nutrient-deprivation autophagy factor 1 (NAF-1, CISD2, Miner1, ERIS), that primarily localizes in the endoplasmic reticulum (ER) or the mitochondrial associated membrane (MAM) and regulates cell autophagy, and could potentially be another anti-diabetic drug target (38-40). A missense mutation in NAF-1 is responsible Wolfram Syndrome 2, a rare, autosomal recessive neurodegenerative disease (40-43). High expressions of NAF-1 is also a dependent factor for tumorigenicity in breast cancer (44). A deficiency in cellular NAF-1 is also shown to cause premature aging (45).

### 1.3 Third member of human NEET protein MiNT

The focus on this thesis will be another homolog in the human NEET protein family, mitochondrial inner NEET protein (MiNT, CISD3, Miner2). Sequence and structural

comparison of MiNT in comparison to mNT and NAF-1 is shown below in **Figure 1.2** & **Figure 1.3** showing the domains of the signature CDG(S/A/T)H sequence that can be found in all NEET proteins (40, 46-48).

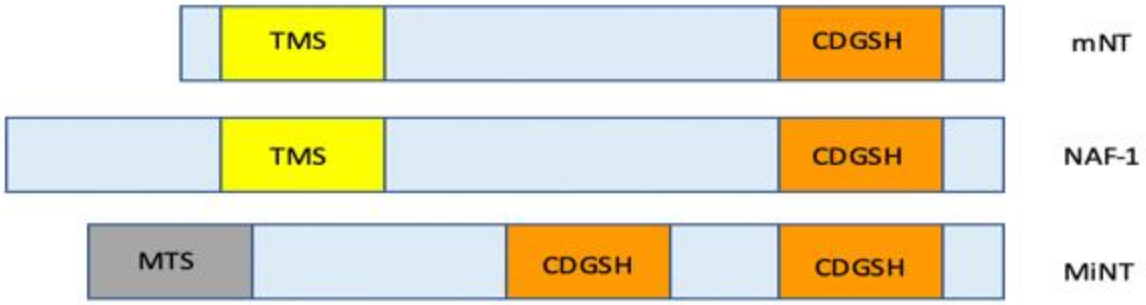


**Figure 1.2**: **General amino acid sequence alignment of three human NEET proteins.** This figure shows the sequence organization between the monomeric MiNT versus the dimeric mNT and NAF-1 with CDGSH domains shown. TMS refers to the transmembrane sequence and MTS refers to the mitochondrial targeting sequence of MiNT, which is cleaved upon transport into the mitochondria. Both mNT and NAF-1 are homodimers, and MiNT is a monomer.

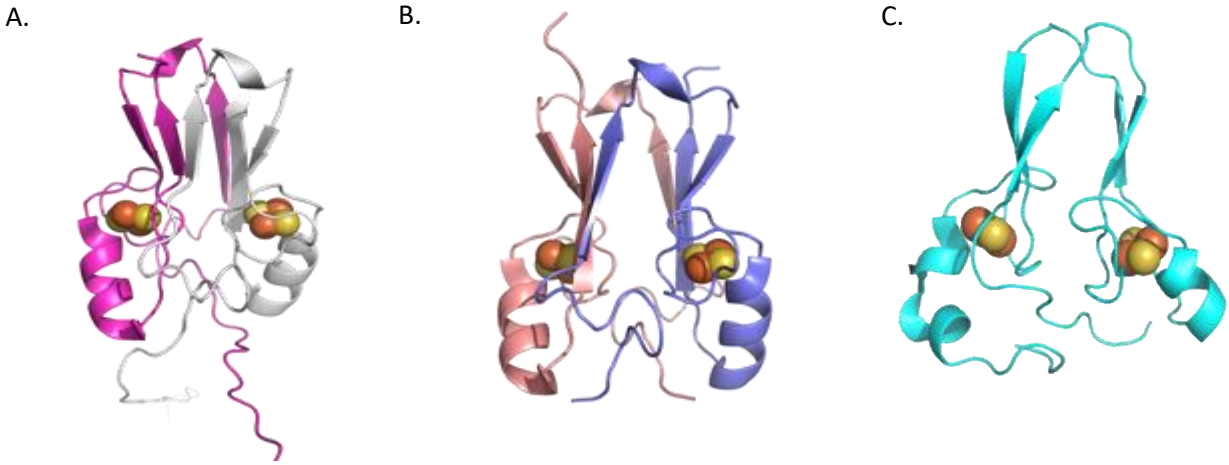


**Figure 1.3: Crystal structure of the human NEET proteins.** A. WT mNT (PDB no: 3EW0), the two promoters that constitute the dimeric fold are colored in magenta and grey, respectively. B. WT NAF-1 (PDB no: 3FNV) the two promoters that constitute the dimeric fold are colored in salmon and slate, respectively. C. The monomeric all Cys mutant MiNT (PDB no: 6AVJ). Yellow spheres depict the inorganic sulfur atoms and the orange spheres show iron atoms.

Like mNT and NAF-1, MiNT possesses both the beta cap domains and cluster binding domains, a signature structures in the NEET-family fold (49). However, from the sequence and structural differences in **Figure 1.2** and **Figure 1.3**, it can be seen that MiNT is a monomeric NEET protein containing 2 CDGSH domains in the protomer as opposed to the homodimeric mNT and NAF-1 containing one CDGSH domain per protomer (48). MiNT is considered as a type 5/6 CISD protein based on the motifs in a comparison study of CISD proteins in prokaryotes and eukaryotes (50). Also, the cluster binding sites are different in MiNT based on the sequence differences (**Table 2.1**). Pertaining to its name, MiNT localizes within the mitochondrial matrix, however; MiNT lacks the transmembrane domain sequence common to mitoNEET and NAF-1 (48, 51). Even though many studies of mNT and NAF-1 exist, little information about MiNT function has been describe thus far. What is known is that MiNT is overexpressed in many cancer cells (48, 52). MiNT has been identified recently on its upregulated expression towards chronic obstructive pulmonary disease (COPD), a leading cause of death globally (53, 54). MiNT is also a potential candidate for nitric oxide signaling by stabilization of the iron-sulfur cluster while exposed with nitric oxide in anaerobic conditions (55). This is in opposition to the expected effect based on the typical result of modification and destabilization of iron-sulfur clusters when exposed to NO (56, 57). Our lab has conducted cluster transfer studies using human ferredoxin 1/ adrenodoxin (FDX1) and human ferredoxin 2 (FDX2) as transfer acceptor partners by comparing the rate of a holo-MiNT loss of cluster absorption at 458 nm, concomitant with the formation of holo-FDX from apo-FDX by monitoring the change in the characteristic 420 nm absorbance against time indicating the similarities in cluster transfer between MiNT versus mNT and NAF-1 (48). An absence of MiNT can also result in an accumulation of free labile iron and ROS, as seen in a confocal study using two different cancer cell lines suppressing MiNT expression (48). This suggest that MiNT also regulates free labile iron, matching general characteristics with mNT

and NAF-1. Due to its asymmetry as a result of sequence and structural differences in the two cluster-binding halves of the protein, MiNT can possess characteristics that may not be seen in the C2 symmetric homodimeric human NEET protein. Investigations of the physical and chemical properties of MiNT is of great interest in order to find out the exact roles within the ISC pathway in iron trafficking or that it could be potentially a novel drug target.

### 1.4 Present analysis on MiNT

We are currently interested in the characteristic investigation of MiNT since not much is known about it. Chapter 2 and 3 talks about the general purification and assays employed to achieve that. Chapter 4 will reveal new characteristics not known to human NEET protein so far due to the consequences the asymmetry of the two cluster binding sites by using biophysical assays like ultra-violet visible spectroscopy (UV-Vis) and circular dichroism (CD) comparison studies. UV- Vis spectroscopy is employed as both quantitative and qualitative assay for MiNT while CD spectroscopy is applied in order to study the secondary structure of MiNT more carefully, as the only current structural reference to the WT MiNT is through double mutant crystal structure of MiNT. Application of the results in the subsequent chapters will serve as a foundation for further studies by providing further insight into the function of NEET proteins.

# Chapter 2

# General Methods

## 2.1 Introduction

The increasing importance in the role of Mitochondria inner NEET protein (MiNT) has recently been recognized in cancer (48). However, not much is known about MiNT in comparison to the more well-known homologous NEET protein mitoNEET (mNT) and nutrient-depravation autophagy factor-1 (NAF-1). mNT and NAF-1 are known as homodimers while MiNT is monomeric containing two cluster binding sites (48). In order to understand the Iron sulfur (2Fe-2S) cluster characteristics of MiNT due to its asymmetry, single point mutations are done in order to achieve four different constructs, mainly changing the histidine ligand to cysteine in position 75 and 113 respectively, a double mutant protein and compared to the WT construct. A previous study from our lab indicates that mutation of the histidine ligand to a cysteine ligand resulted in higher stability of the iron sulfur cluster in mNT (58). One construct set contains the 6-histidine tag (His-tag) on the carboxyl terminal (C-Terminal) and another set does not (**Table 2.1**). The various construct plasmids were transformed into the appropriate strain of the bacteria *Escherichia coli* (*E. coli*) for expression. Purification steps are required to isolate and maintain the integrity of the protein, which can be subsequently used to run biophysical assays for characterization such as UV-Vis spectroscopy and CD. Sodium dodecyl sulfate poly acrylamide gel electrophoresis (SDS-PAGE) and liquid chromatography-mass spectrometry (LC-MS) are run to confirm whether the purification steps has yielded the protein with the correct, expected molecular weight and a high-degree of purity. General methods are further described below to avoid repetition in the remainder of this thesis.

**Table 2.1: Amino acid sequence of MiNT (36-127) with highlighted single point mutations for each construct**. Mutations were made at positions 75 and 113 respectively or both. Histidine, cysteines and his-tag sequence are color coordinated for clarification.

| Tagged Construct of MiNT | Sequence |
|---|---|
| **WT-tag** | MPARSVVALK TPIKVELVAG KTYRWCVCGR SKKQPFCDGS HFFQRTGLSP LKFKAQETRM VALCTCKATQ RPPYCDGTHR SERVQKAEVG SPL LEHHHHHH |
| **H75C-tag** | MPARSVVALK TPIKVELVAG KTYRWCVCGR SKKQPFCDGS CFFQRTGLSP LKFKAQETRM VALCTCKATQ RPPYCDGTHR SERVQKAEVG SPL LEHHHHHH |
| **H113C-tag** | MPARSVVALK TPIKVELVAG KTYRWCVCGR SKKQPFCDGS HFFQRTGLSP LKFKAQETRM VALCTCKATQ RPPYCDGTCR SERVQKAEVG SPL LEHHHHHH |
| **Double mutant-tag (DM-tag)** | MPARSVVALK TPIKVELVAG KTYRWCVCGR SKKQPFCDGS CFFQRTGLSP LKFKAQETRM VALCTCKATQ RPPYCDGTCR SERVQKAEVG SPL LEHHHHHH |
| | |
| **Non-Tagged Construct of MiNT** | |
| **WT** | MPARSVVALK TPIKVELVAG KTYRWCVCGR SKKQPFCDGS HFFQRTGLSP LKFKAQETRM VALCTCKATQ RPPYCDGTHR SERVQKAEVG SPL |
| **H75C** | MPARSVVALK TPIKVELVAG KTYRWCVCGR SKKQPFCDGS CFFQRTGLSP LKFKAQETRM VALCTCKATQ RPPYCDGTHR SERVQKAEVG SPL |
| **H113C** | MPARSVVALK TPIKVELVAG KTYRWCVCGR SKKQPFCDGS HFFQRTGLSP LKFKAQETRM VALCTCKATQ RPPYCDGTCR SERVQKAEVG SPL |
| **DM** | MPARSVVALK TPIKVELVAG KTYRWCVCGR SKKQPFCDGS CFFQRTGLSP LKFKAQETRM VALCTCKATQ RPPYCDGTCR SERVQKAEVG SPL |

## 2.2 Methods

### 2.2.1 Transformation protocol

In order for proteins to be expressed, plasmids are transformed into a competent *E. coli* cells which are designed for foreign DNA incorporation in this transformation step. 2 μL plasmids containing WT or mutant genes are first added to 50 μL of thawed competent cells on ice. The reaction is allowed to stand on ice for 30 minutes and heat shocked at 42 ºC for 45 seconds. The reaction is placed back on ice while 500 μL of pre-warmed sterile Super Optimal broth with Catabolite Expression (S.O.C) (Thermo Fisher Scientific) is added sterile 15 mL falcon tube. All of the transformation reactions are transferred into the S.O.C and are allowed to grow at 37 º C for one hour in a shaker at 225 rpm. The whole amount is then transferred into a 1.7 mL sterile Eppendorf tube and centrifuged at 5000 x g for one minute. The supernatant is discarded leaving the pellet (competent cells that contain the plasmid). 20 μL of autoclaved milliQ water is added to the pellet portion in the tube and are mixed well. The cells in water are then pipetted to Luria-Bertani (LB) agar with the appropriate antibiotics and grown overnight at 37 º C.

### 2.2.2 Construction and verification of plasmids

A plasmid that contained MiNT sequence of 36-127 had been previously cloned into a pet 24a vector containing a kanamycin (kan) resistance gene in between NdeI and Xhol region. In order to verify its sequence, it was transformed to a competent DH5-Alpha *E. coli* cells (DH5α) (Invitrogen) for cloning applications. The transformation is as described above. The cells were grown in 15 mL LB media with kan (50 μg/mL) (Fisher Bioreagents) overnight at 37 º C and centrifuged down with 4000 x g in 4 º C. Supernatants were discarded, leaving the cell pellets. DNA Plasmid Miniprep Kits (Invitrogen) reagents and spin columns were used to lyse the cells and collect the high-copy DNA. Most of the steps can be found as described with

minor changes (59). Resuspension buffer (R3), Lysis buffer (L7) and Precipitation Buffer (N4) volumes were doubled to efficiently lyse cells that results from 15 mL of growth, rather than the 5 mL used in the standard protocol. Also, TE buffer volume was changed to 40 µL instead of 70 µL to get a high enough concentration of DNA for sequencing (Eton Bioscience Inc). Concentrations of the DNA were determined by using Nanodrop ND-1000 Spectrophotometer in ng/µL at 260 nm. Example amino acid sequence of the Wild Type (WT) was verified as shown below (**Figure 2.1**).

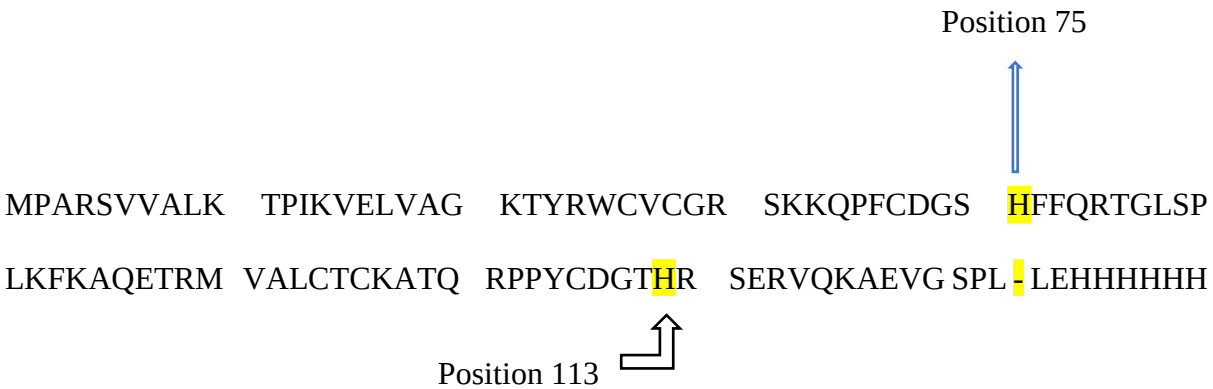


**Figure 2.1: Sequence of WT MiNT.** Amino acid sequence of the Wild type MiNT after sequencing and verification using SnapGene Viewer and Expasy. The dash before the His-tag refers to a stop codon.

In order to make constructs with the His-tag, a stop codon deletion step mutation was performed. Thereafter, a substitution mutation was performed at position 75 and 113 individually, then for both simultaneously. For non-His-tagged constructs, this deletion step was not necessary. All of the mutations were performed using Polymerase Chain Reaction (PCR) and primers were designed using QuickChange Primer Design (Agilent) as shown on the table below (**Table 2.2**).

**Table 2.2**: **Designed primers for deletion and substitution mutations.**

| Primer Type | Sequence | Melting Temperature (℃) |
|---|---|---|
| Deletion Primer F | ggctccccactcctcgagcaccac | 67.3 |
| Deletion Primer R | gtggtgctcgaggagtggggagcc | 67.3 |
| H75C Primer F | ccttctgtgacggctcctgcttcttccaacgcactg | 69.0 |
| H75C Primer R | cagtgcgttggaagaagcaggagccgtcacagaagg | 69.0 |
| H113C Primer F | actgcgatggcacctgcaggagtgagcgcg | 71.4 |
| H113C Primer R | cgcgctcactcctgcaggtgccatcgcagt | 71.4 |

**Table 2.3**: **Recipe for PCR sample reactions with various amounts of double stranded DNA.**

| Amt of Template DNA (ng) | 5 | 10 | 25 |
|---|---|---|---|
| **Reactants** | | | |
| **Reaction Buffer (uL)** | 5 | 5 | 5 |
| **Plasmid (uL)** | 2 | 4 | 10 |
| **Forward Primer(uL)** | 1 | 1 | 1 |
| **Reverse Primer(uL)** | 1 | 1 | 1 |
| **dNTP(uL)** | 1.1 | 1.1 | 1.1 |
| **Water(uL)** | 39.9 | 37.9 | 31.9 |
| **Taq Polymerase(uL)** | 1 | 1 | 1 |

Forward and reverse primers were purchased from Eton Bioscience, Taq polymerase and reaction buffer were purchased from Agilent, and restriction enzyme DPN1 was purchased from New England Biolabs. The verified sequence plasmid with measured concentrations using Nanodrop was first diluted to a final concentration of 2.5 ng/μL before adding other reactants as shown in Table 2.3. The forward and reverse primers were diluted with milliQ water to 125 ng /μL for calculation convenience. The reactants were added into a PCR tube on ice, and then transferred to C1000 Touch Thermal Cycler (Biorad). PCR contains three steps, denaturing, annealing and extending for amplification of DNA to be achieved. Thus, the program in the Thermal Cycler was set as shown below (Table 2.4).

**Table 2.4**: **Program used for thermal cycler**. Repeat the 5th step 16 times for single point mutations and 18 times for deletion. Tm is the melting temperature of primer for determining the cycle temperature.

| Steps | Segment | Temperature(°C) | Time(min) |
|---|---|---|---|
| **Initial Denature** | 1 | 98 | 2.0 |
| **Cycle Denature** | 2 | 98 | 0.75 |
| **Annealing** | 3 | Tm - 5.0 | 1.0 |
| **dNTP arrangement** | 4 | 72 | 7.0 |
| | 5 | Repeat | |
| **Extension** | 6 | 72 | 10 |
| | 7 | 4.0 | Unlimited |

After PCR was completed, 1 μL of DPN1 was added to the reaction to digest parental/ non-mutated DNA and was incubated at 37 º C for at least one hour before storing it at -20 º C. Mutated constructs would then be transformed into DH5α cells grown in LB agar plates with kan and steps above were repeated to verify the mutated sequence.

### 2.2.3 Expressions checks and glycerol stocks

The verified sequences of WT and mutants were transformed into a BL21(DE3)-RP competent cell (Agilent). This strain of *E. coli* was chosen as it was optimized for rare codons for arginine (R) and proline (P), important in the case of the DNA sequence for MiNT. BL21(DE3)-RP cells generally contains a plasmid that has chloramphenicol (cam) resistance. In order to ensure that the growth of cells contains the plasmid (with kanamycin resistance), LB media must contain both kan (30 μg/mL) and cam (30 μg/mL)(Thermo Fisher). To begin, transformed cells with each DNA construct (Table 2.1) were grown overnight at 37 º C in 5 mL of LB media (kan + cam). The overnight cells were divided into two tubes containing 10 mL of LB media (kan + cam) with each having 1:10 dilution. One was for glycerol stock, the other was for expression check. For the glycerol stock fraction, it was allowed to grow at 37 º C until the Optical Density (OD) reading using UV-Vis spectroscopy (UV-Vis) (Biorad

SmartSpec Plus) reached 0.5 at 600 nm. A 1 mL glycerol stock would be made by adding the cells to Glycerol with a ratio of 1:1. The glycerol stock would be stored at -80 ºC. For the expression check fraction, the cells were allowed to grow at 37 º C until the OD reached 0.8. 200 µL of cells would be collected and centrifuged at 10000 x g for 1 minute, discarding the supernatant and stored at -20 ºC. This fraction was identified as the non-induced fraction. Isopropyl β-D-1-thiogalactopyranoside (IPTG) (Teknova) of 1 mM concentration was added into the expression check fraction and further grown at 37 ºC for another 6 hours. 200 µL of cells would then be collected after the 6-hour mark and centrifuged, discarding the supernatant and stored in -20 ºC. This fraction was identified as the induced fraction. SDS-PAGE gels were run to confirm the expression of the protein by comparing the non-induced fraction and the induced fraction.

### 2.2.4 SDS-PAGE

Since the molar weight of WT construct is about 10.4 kDa, a 15 % bis-acrylamide SDS – PAGE was chosen for better resolution. This was made by using the recipe as shown below.

**Table 2.5**: **List of reactants and volumes to make 15 % acrylamide SDS-PAGE gel**.

| Resolving Gel (15 mL) | Volume | Stacking Gel (5 mL) | Volume |
|---|---|---|---|
| **1.5 M Tris pH 8.8** | 5.0 mL | **0.5 M Tris pH 6.8** | 0.62 mL |
| **30% Acrylamide** | 7.5 mL | **30% Acrylamide** | 0.83 mL |
| **Water** | 2.4 mL | **Water** | 3.82 mL |
| **20% SDS** | 75 uL | **20% SDS** | 25 uL |
| **10% APS** | 75 uL | **10% APS** | 50 uL |
| **TEMED** | 25 uL | **TEMED** | 5.0 uL |

For pellet samples, 50 µL of 2 X loading buffer and 1 µL *β-mercaptoethanol (BME) (Biorad)* were added into the cell. For non-cell contained samples, a 3:1 sample to 2x loading buffer ratio was made with the additional 1 µL of *BME*. They were then boiled to at least 85 ºC for a few minutes until condensation can be seen from the tube cover. Boiled samples were removed to allow cooling. Then, 10 µL of each sample was used to fill each well and an extra well was left for 8 µL of G02101 Accuruler Pre-stained Protein Ladder (Lambda Biotech) for size comparison standard. The process was run at 120 V for about 1.5 hour. Gel photographs were taken either by a personal camera or a gel imager (Syngene Ingenius).

### 2.2.5 Growth of cells and purification of proteins

For both His-tagged constructs and non-His-tagged constructs, the procedure of bacteria growth were the same. A 200 mL LB media containing kan and cam was used to grow the cells overnight at 37 ºC with a speed of 180 rpm. The overnight cells were then divided into three for transferring into a 2 L of LB media each containing kan and cam and were allowed to grow until OD reached 0.8. After optimization, it was determined that 0.5 mM IPTG would be used to induce the cells at 18 ºC for 18 hours. Cell pellets were collected using centrifugation (Avanti Centrifuge J-20XP) with JLA-8.1000 rotor (Beckman) at 3000 rpm and 4 ºC. The pelleted cells were added with 50 mL of lysis buffer containing 50 mM Tris (Sigma Life Science) pH 8.0 and 50 mM NaCl (Fisher Chemical) and was stored at -80 ºC and left for a day before purification.

*Purification of His-tagged MiNT constructs*

Frozen cells were thawed and 1mM of phenylmethylsulfonyl fluoride (PMSF) was added to inhibit proteases. The solution was then sonicated using 550 Sonic Dismembrator (Thermo Fisher) programmed for a 5 second pulse and 15 seconds off for a total of 10 minutes. The lysed solution was transferred to a 50 mL tube and centrifuged using JA-20 rotor (Beckman) at 15,000 rpm and 4 ºC for 30 minutes. The supernatant fraction was poured into a $Ni^{2+}$-NTA agarose (Qiagen) column pre-equilibrated with 50 mM Tris pH 8.0 and 350 mM NaCl in a 4 ºC room. The mixture was allowed to incubate for a few minutes for the proteins to fully bind onto the resin. Flow through was collected by gravity filtration. Wash buffer 1 containing 50 mM Tris pH 8.0, 350 mM NaCl and 5 mM imidazole is used for initial washing. Wash buffer 2 containing 50 mM Tris pH 8.0, 350 mM NaCl and 40 mM imidazole is used for subsequent wash. Elution buffer containing 50 mM Tris pH 8.0, 350 mM NaCl and 500 mM imidazole is then added and left to sit for a few minutes to outcompete the His-tag from the resin and was eluted by collecting the flow-through with this wash buffer. The elution fraction is buffer exchanged to lower the concentration of NaCl and imidazole before separation by Fast Protein Liquid Chromatography (FPLC) using Biorad NGC Chromatography system. HiTrap SP HP cation exchange chromatography column (GE Healthcare Life Sciences) is used with the FPLC step as the isoelectric point (pI) of protein is ~ 9.7. The program is set to run an elution gradient from 30 mM NaCl to 600 mM NaCl. Buffers A and B contain 50 mM Tris pH 8.0 and 50-mM Tris pH 8.0 + 1M NaCl respectively. Eluted fractions containing MiNT red in color are pooled and further concentrated, flash frozen with liquid nitrogen (Airgas) and stored at -80 ºC. SDS-PAGE gel electrophoresis is used to assess the purity of the fractions.

*Purification of Non-His-tagged constructs*

Frozen cells are thawed and 1 mM of PMSF is added into the mixture. Cell pellets are diluted up to 100 mL of lysis buffer (50 mM Tris pH 8.0 + 50 mM NaCl) before using the Avestin Emulsiflex – C5 High pressure Homoginizer (ATA Scientific). After homoginizing, 40 μL of Deoxyribonuclease I (DNase I) (New England Biolabs) and 2 mM $MgCl_2$ are added and the mixture is incubated at room temperature for 20 minutes. After incubation, the mixture is transferred to a 50 mL tube and centrifuged at 15,000 rpm and 4 ºC for 45 minutes. The lysate supernatant is collected and filtered with a 33 mm diameter 0.22 μm syringe filter unit (Millipore) twice. Lysate supernatant was injected into the FPLC machine and purified with cation exchange another three times stepwise. Buffer A and B conditions are the same as before but with 5 mM dithiothreitol (DTT) (Biopioneer). The first two sets of cation exchange were run isocratic at 360 mM NaCl after a column wash step, while the third cation exchange was run using a gradient from 30 mM NaCl to 600 mM NaCl. MiNT and its mutants typically elute at between 350 mM to 370 mM NaCl. The fractions from the third ion exchange run were concentrated to less than 10 mL for loading in the size exclusion column. HiPrep 26/60 Sephacryl S-100 High Resolution (S100) (GE Healthcare Life Sciences) is used for this size exclusion step. The buffer used to run the size exclusion column contained 50 mM Tris pH 8.0, 150 mM NaCl and 5 mM DTT. The elution fraction is then combined and concentrated and buffer exchanged several times to remove the DTT. The concentrated protein sample was flash frozen and placed in -80 ºC. SDS PAGE analysis confirmed the efficiency of each step. 15 μL of each sample (WT and DM) were sent for Liquid-Chromatography Mass Spectrometry (LC-MS) using Phenomenex Aeris Widepore XB-C18 column to further confirm purity as well as the efficiency of size exclusion columns. Concentrations of the purified protein were assayed for concentration using Nanodrop at 458 nm.

## 2.3 Biophysical assays and analysis

*UV-Vis Spectroscopy*

Stability assays were carried out using Cary 50 Bio (Varian) spectrometer connected to a CFT-25 Refrigerated Recirculation water bath. Samples of oxidized protein (20 μM) were typically in buffer that contained 50 mM Tris pH 8.0 and 150 mM NaCl. Assays were performed at 37 ºC and 25 ºC respectively. 1 cm pathlength cuvette (Spectrocell) were used for sample analysis. An additional 100 μL of paraffin oil (Hampton Research) was added to the top of the sample to prevent evaporation and condensation. For a reduced sample, 30 μM of protein was also prepared in the buffer as mentioned above, but with an additional 15 mM DTT. This assay was run in 15 ºC without paraffin oil.

*CD Spectrometry*

Runs of CD Spectra in the range of 300 nm to 800 nm were collected using Jasco J-815 Spectrometer. Samples of 30 μM protein were in buffer containing 50 mM Tris pH 8.0 and 150 mM NaCl in a 1 cm pathlength cuvette. A Peltier temperature controller was also used to achieve a 15 ºC run. Spectrum measurement program was used to collect the data with the parameters with a data pitch of 1 nm, a 50 nm/min scanning speed, and 1 nm of bandwidth. Scans were typically averaged over four runs. The Spectra Analysis program was used to analyze the spectra.

For ranges of near to far UV-range at 200nm to 300 nm, a Circular Dichroism Spectrometer Model 215 (Aviv Instruments Inc) was used to typically check the overall shape of the protein with mutations. Sample conditions were the same as mentioned above but a 0.1 cm pathlength cuvette (Spectrocell) was used and data were collected at 15 ºC. The Aviv instrument software was used to collect and export data.

# Chapter 3

## MiNT: Effects of a C-terminal Histidine Tag and Purification Efficiency of WT and Mutants

## 3.1 Introduction

The objective of recombinant protein purification is to yield the maximum amount of protein possible while maintaining its structural and functional integrity. The sequence of MiNT construct of position 36 to 127 previously subcloned into pet 24a vector, is as shown in **Figure 2.1**. A few factors in regards to the recombinant protein construct and the purification protocol have to be considered. Combining the fact that there is a 6-histidine tag (His-tag) sequence readily available in the plasmid construct and that it is widely believed that His-tag will not affect the overall function of the protein leads to the decision to use tagged construct of MiNT as shown in **Table 2.1** (60, 61). However, this was not optimal in this case. Issues with the purification process of MiNT and troubleshooting will be thoroughly discussed.

## 3.2 Results and discussion

**Table 3.1**: **Constructs of MiNT showing the molecular weight without 2Fe-2S clusters and the isoelectric point.**

| Constructs | Molecular Weight (kDa) | Isoelectric Point (pI) |
|---|---|---|
| **WT-tag** | 11.33 | 9.74 |
| **H75C-tag** | 11.30 | 9.64 |
| **H113C-tag** | 11.30 | 9.64 |
| **Double Mutant-tag** | 11.27 | 9.54 |
| | | |
| **WT** | 10.27 | 9.87 |
| **H75C** | 10.24 | 9.76 |
| **H113C** | 10.24 | 9.76 |
| **Double Mutant** | 10.20 | 9.66 |

A previous study showed that a single point mutation, typically a histidine to cysteine involved in cluster ligation, does not affect the globular structure of the protein (62). In the case of mNT a cysteine mutant results in a more stable cluster structure that retains pH sensitivity

(58, 63). **Table 3.1** shows the relative molecular weight and isoelectric point which will prove useful in the purification step considerations. Studies also show that NEET proteins are likely to be more stable at higher pH (40). Therefore, purification buffers are usually set at pH 8.0 or above, as is the case here.

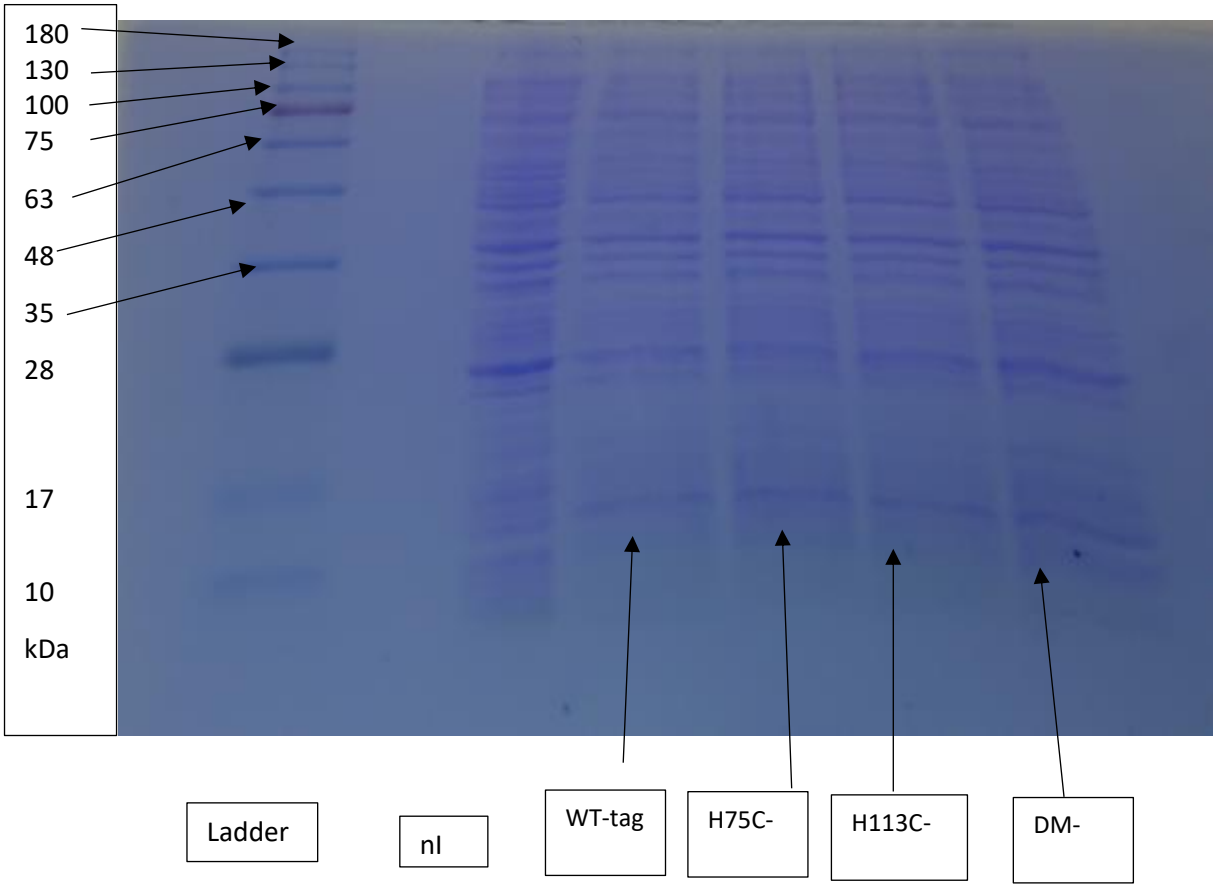


**Figure 3.1: Protein expression for tagged MiNT constructs.** This figure shows the 15% bis-acrylamide SDS-PAGE gel with tagged constructs of samples after pellet collection from centrifugation. nI refers to non-induced fraction and the tagged constructs as shown.

Protein expression for the tagged proteins after transformation are as shown in **Figure 3.1**. Optimal induction conditions were found to be 18 ºC for 18 hours using a final concentration of 0.5 mM IPTG. The reason for adding a His-tag on the construct is to reduce the amount of purification steps to one round of immobilized metal affinity chromatography (IMAC) using Nickel-NTA resin followed by one round of cation exchange column chromatography using fast protein liquid chromatography (FPLC). Without IMAC, injecting

the lysate to the FPLC will be too viscous due to the cell's release of chains of nucleaic acids during lysis (64). The IMAC purification step is able to remove some of the viscosity by trapping negative charges from DNA. One study also suggests that MiNT can possibly be bound to double stranded DNA, protecting the protein from oxidative damage, which makes removal of DNA essential in the purification step to collect only the protein of interest (65). The list of buffers that are used for IMAC is as shown below (**Table 3.2**).

**Table 3.2**: **Concentration of buffer and salts that are used for IMAC.**

| Buffer | Tris pH 8.0 Concentration (mM) | NaCl concentration (mM) | Imidazole Concentration (mM) |
|---|---|---|---|
| **Equilibration** | 50 | 350 | - |
| **Wash 1** | 50 | 350 | 5 |
| **Wash 2** | 50 | 350 | 20 |
| **Wash 3** | 50 | 350 | 30 |
| **Wash 4** | 50 | 350 | 40 |
| **Elution** | 50 | 350 | 500 |

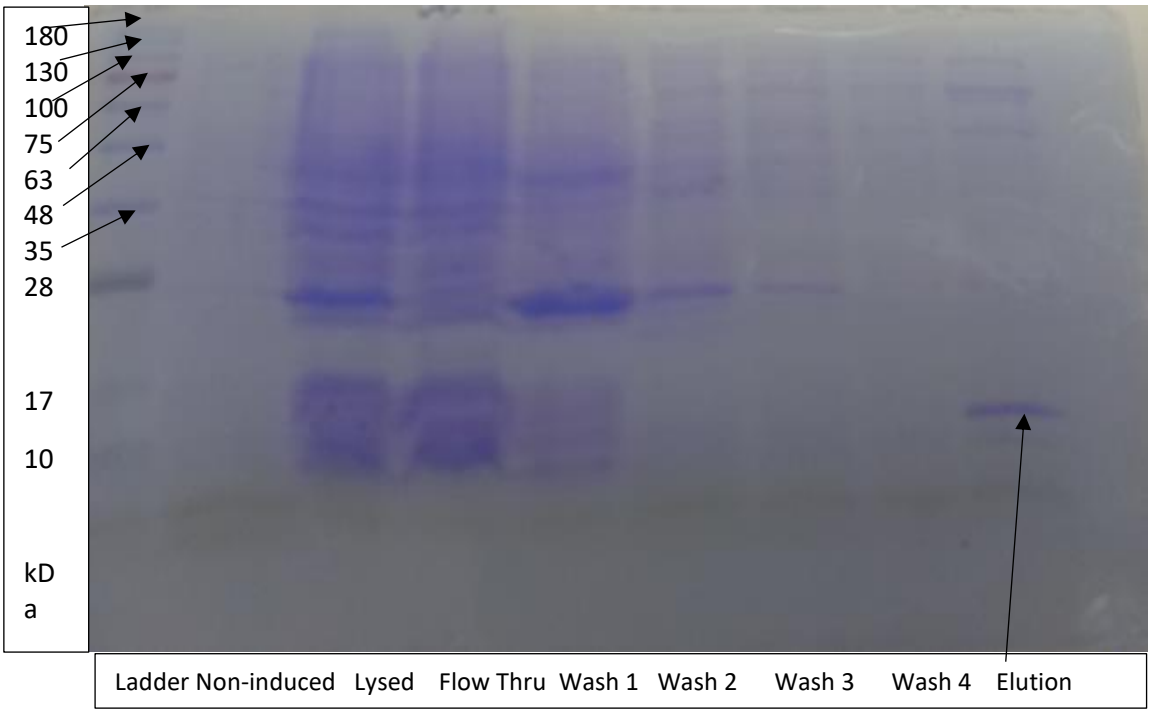


**Figure 3.2**: **15% SDS-PAGE gel of WT-tag construct using IMAC purification.**

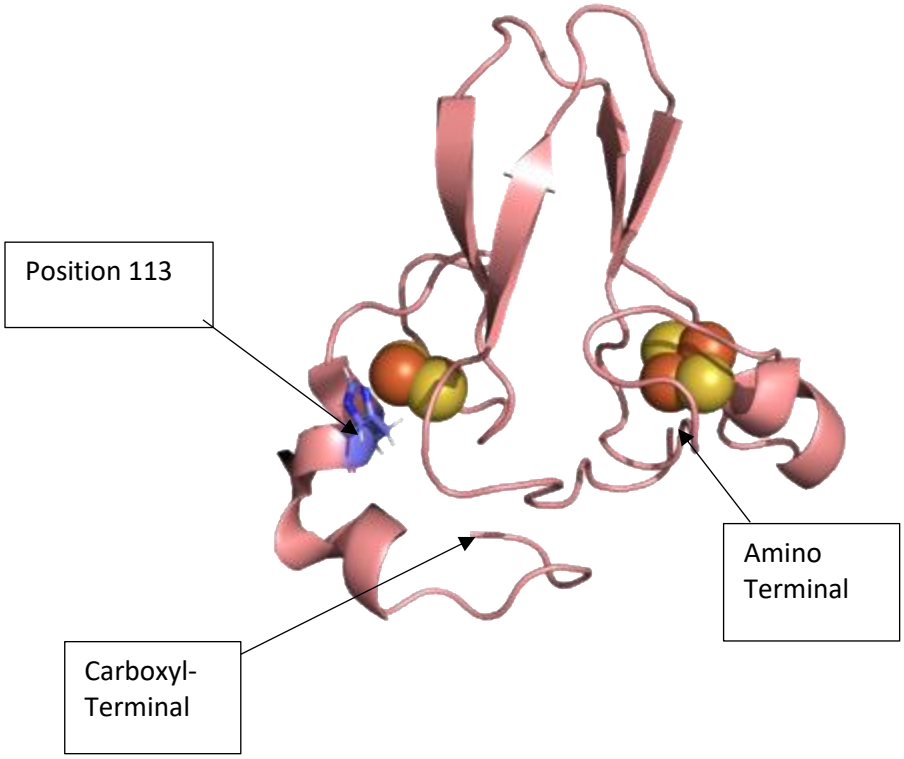


**Figure 3.3**: **Crystal structure of DM MiNT.** Crystal structure of double mutated MiNT (PDB no: 6AVJ) where position 113 is mutated to histidine (slate) using Pymol to show proximity of C terminal and histidine.

Aggregation of tagged-WT constructs are observed in two conditions. One is when the buffer conditions have insufficient NaCl concentration, while the other is during loading into the cation exchange column which requires a precursory concentration step. These observations are opposite of DM-tag protein, which allow further purification step, mainly a cation exchange step using FPLC as shown below (**Figure 3.4)**.

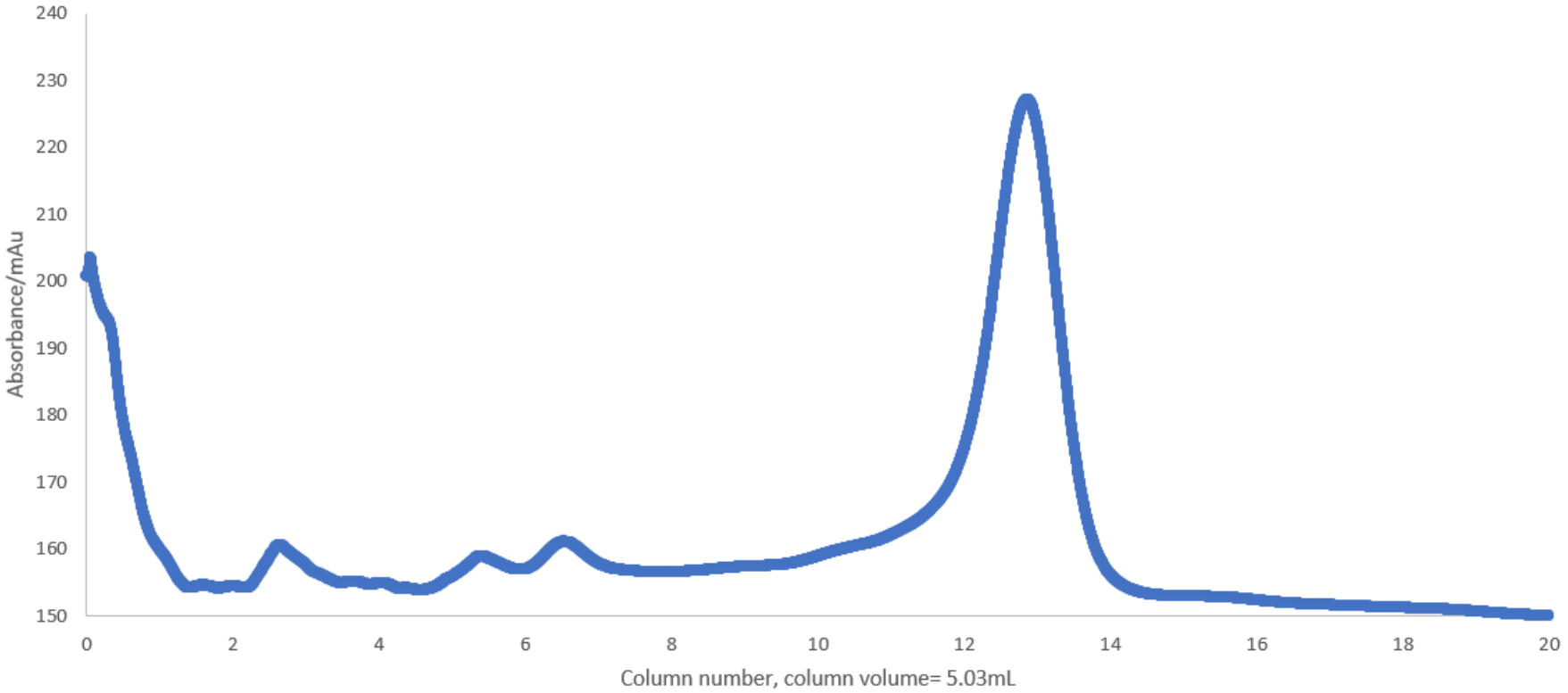


**Figure 3.4**: **Cation exchange purification step for the DM-tagged MiNT construct using a gradient elution from 30 mM to 600 mM NaCl**. The peak of interest is seen from the 12$^{th}$ through the 14$^{th}$ column, which elutes between 300 mM to 330 mM NaCl.

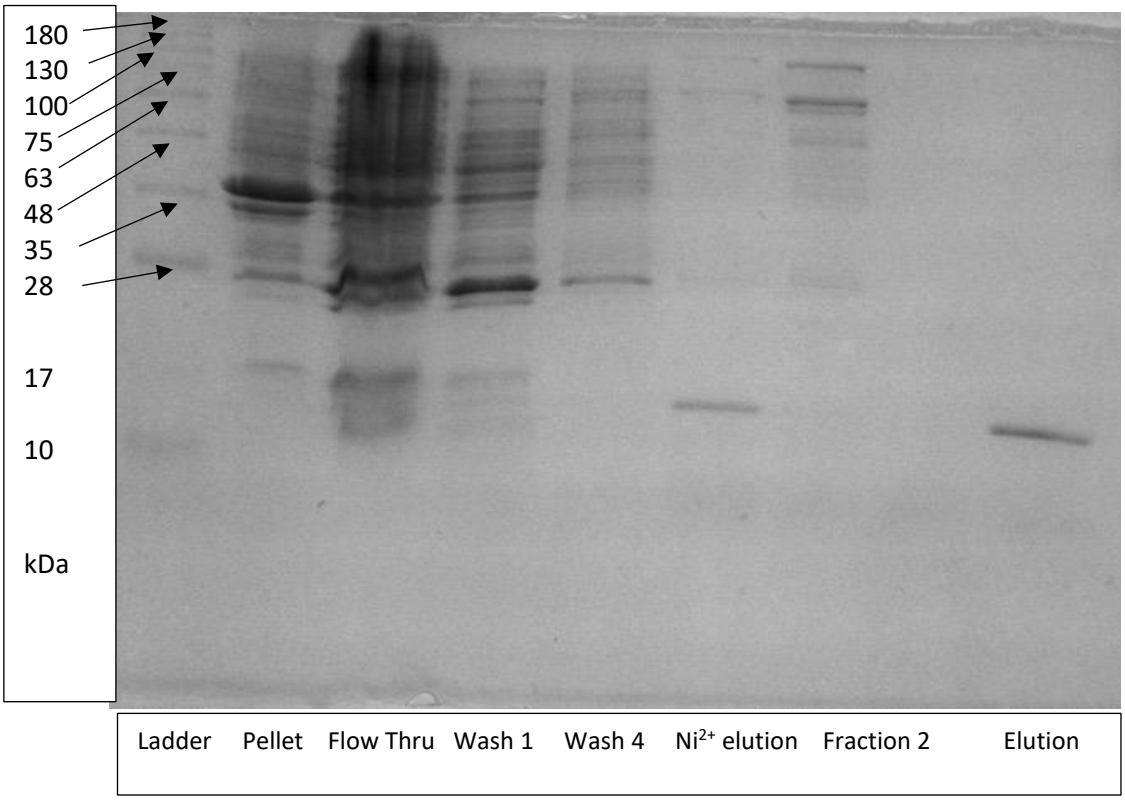


**Figure 3.5**: **SDS-PAGE of DM-tag construct for all purification steps from IMAC to IEX**. Fraction 2 refers to the peak during column wash to check whether any protein of interest eluted out of the column while running gradient elution in FPLC.

**Figure 3.5** shows that the desired level of DM-tag is achieved. Competition of the His-tag against the histidine at position 113 for the iron- sulfur cluster in WT-tag protein can be interpreted from the displacement dynamics (48). Higher iron-sulfur cluster stability in the 4-cysteine ligand does not allow histidine to interfere with the cluster, as can be seen by the success of purification steps of DM-tag. From these results shown above, regardless of whether the His-tag is placed on the C-terminal or the N-terminal of MiNT, it will result in an aggregation in WT MiNT; as intermolecular aggregation can also similarly occur. Despite that for many protein constructs, the His-tag does not affect overall protein function, using a tagged construct is not optimal for MiNT as stability is affected.

Purification steps of a non-tagged construct of MiNT are severely limited. As the lysate is extremely viscous after homogenizing, an excess amount (40 µL of 2000 U/mL stock) of bovine pancreatic deoxyribonuclease I (DNAse I) with 2 mM $MgCl_2$ are added into the homogenate and it is incubated for 20 minutes at room temperature. This ensures that majority of the DNA has been cleaved. Cation exchange is run three times consecutively. An example chromatogram is as shown below for the DM construct elution.

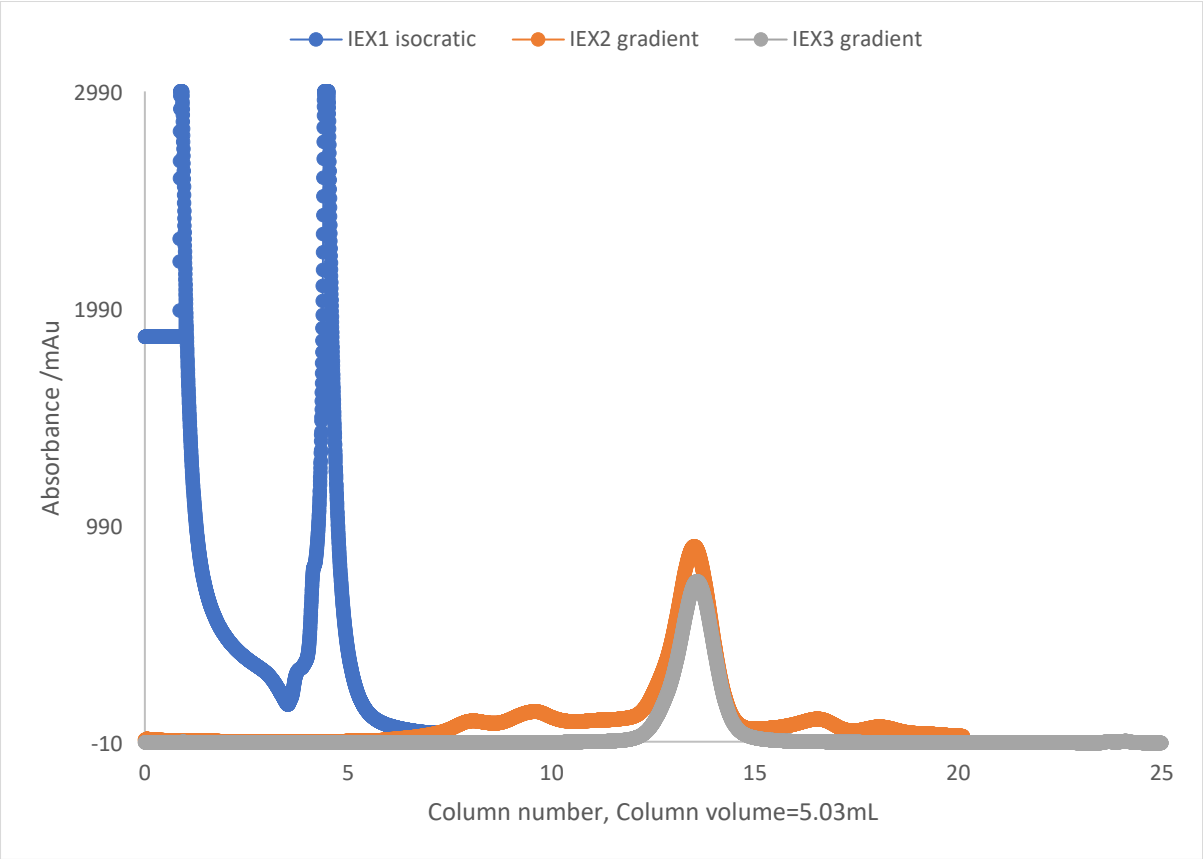


**Figure 3.6**: **FPLC chromatogram of non-tagged DM construct during subsequent IEXs.** The first cation exchange (IEX1) refers to the isocratic concentration of 360 mM NaCl after the initial column wash. The second and third ion exchange (IEX2 and IEX3) refers to a gradient elution program from 30 mM to 600 mM NaCl.

The aim of the first cation exchange is to remove the lysate that does not bind to the column, as well as concentrating the protein of interest into a few elution fractions. The subsequent cation exchange serves to further remove more side proteins that are not close in net charge. Using **Table 3.1**, we can expect similar elution fractions for all non-tagged constructs while performing the third cation exchange as shown below in **Figure 3.7**.

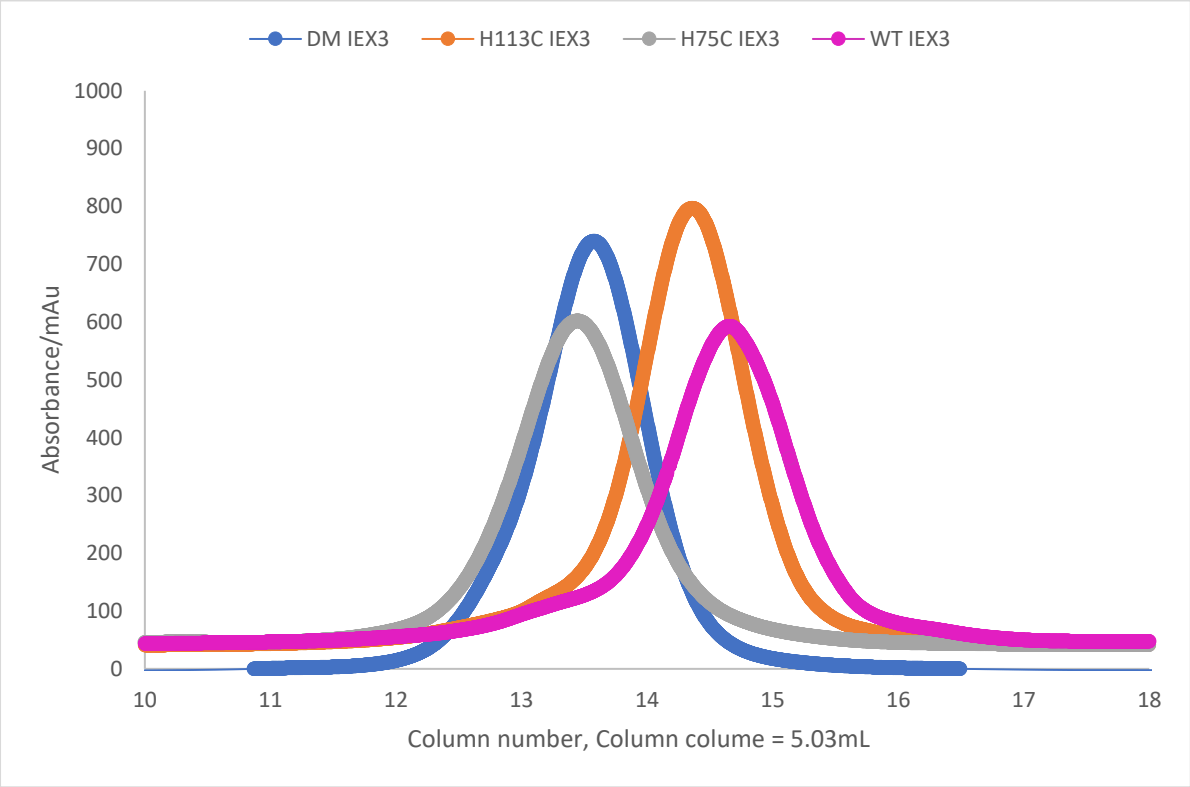


**Figure 3.7**: **Third cation exchange elution fraction of all four, separate non-tagged MiNT constructs**. DM and H75C both elute between 310 mM and 350 mM NaCl, H113C elutes between 330 mM to 370 mM NaCl, and WT elutes between 340 mM to 380 mM NaCl.

A HiPrep 26/60 Sephacryl S-200 HR size exclusion column was initially used for the final purification step for both WT and DM constructs (**Figure 3.8**). However, through liquid chromatography mass spectrometry (LC-MS), the fractions collected were not found to be pure (**Figure 3.9.1 and Figure 3.9.2**) even though an SDS-PAGE analysis suggests that they are (**Figure 3.10**).

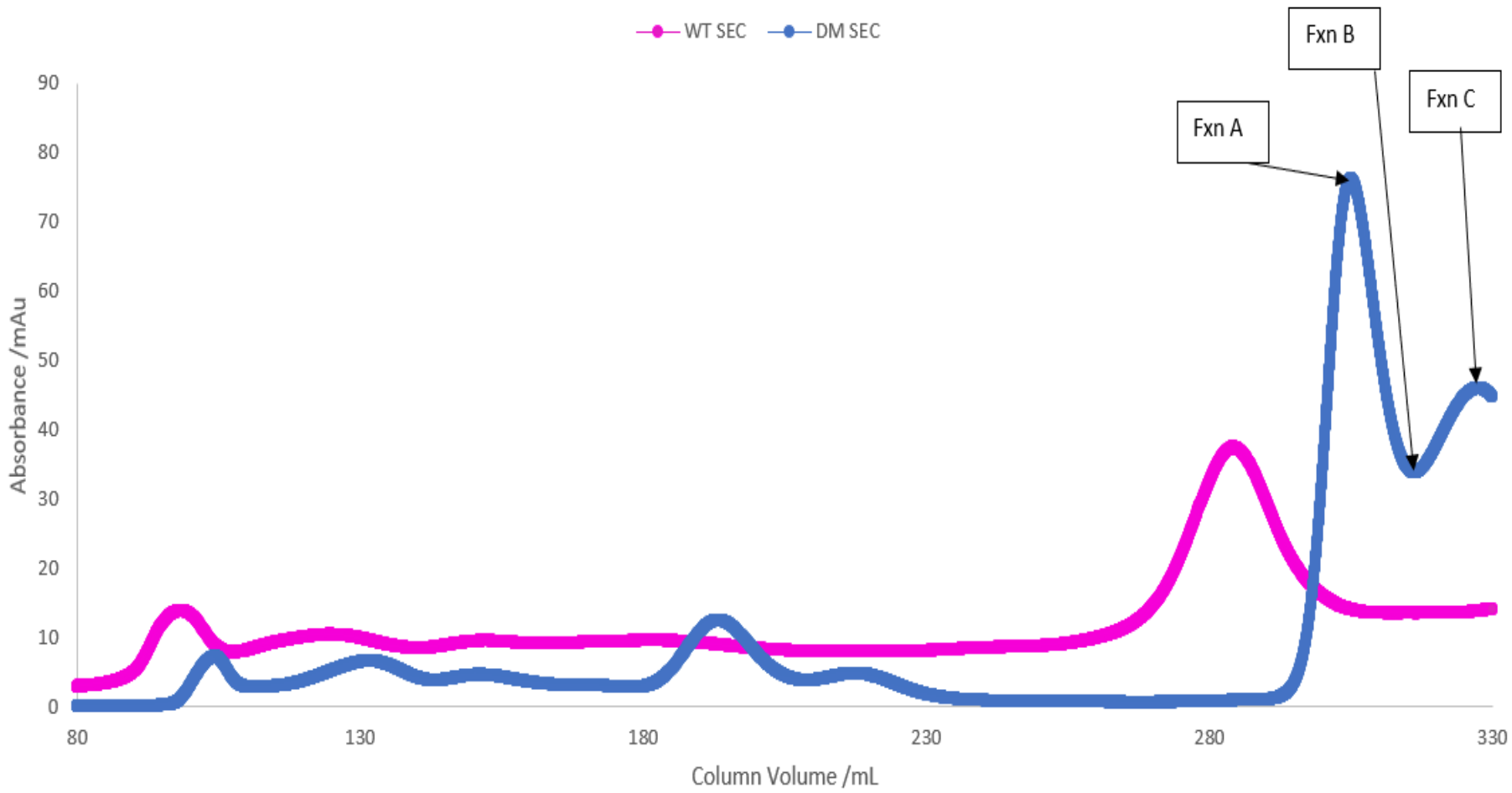


**Figure 3.8**: **Chromatogram of S200 size exclusion column purification step for WT and DM constructs**. Fraction A, B and C (Fxn A, B and C) on DM construct are separated fractions to test for content and purity in SDS-PAGE shown in Figure 3.10.

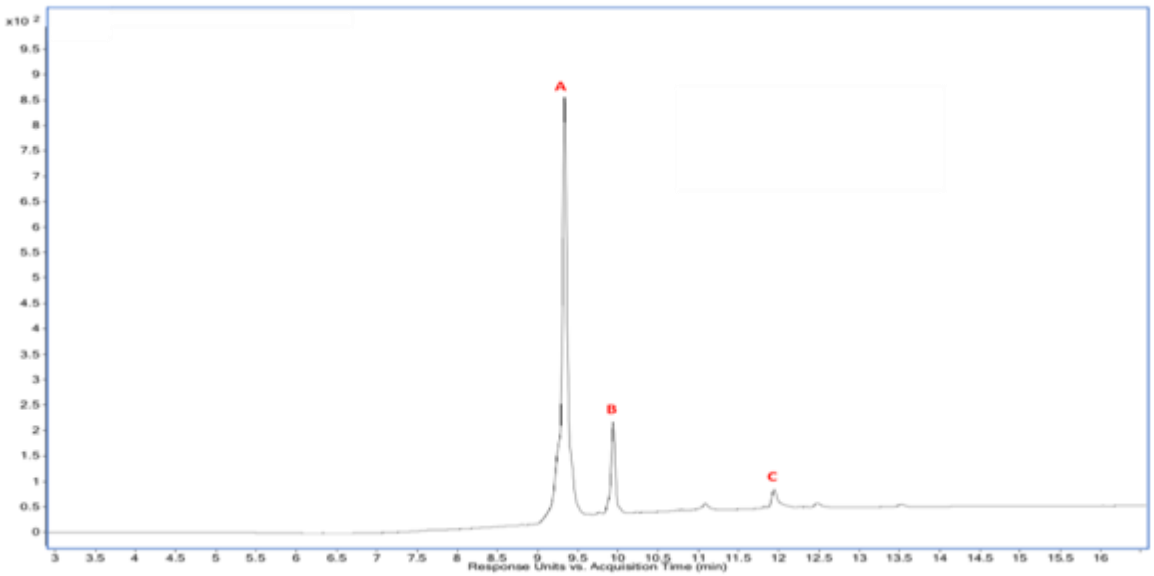


**Figure 3.9.1: Liquid chromatogram in LC-MS using ESI-TOFMS for the purified sample from the S200 non-tagged WT elution**. Trace peak A corresponds to 10268 Da, Trace B 6410.5 Da and Trace C 12606 Da.

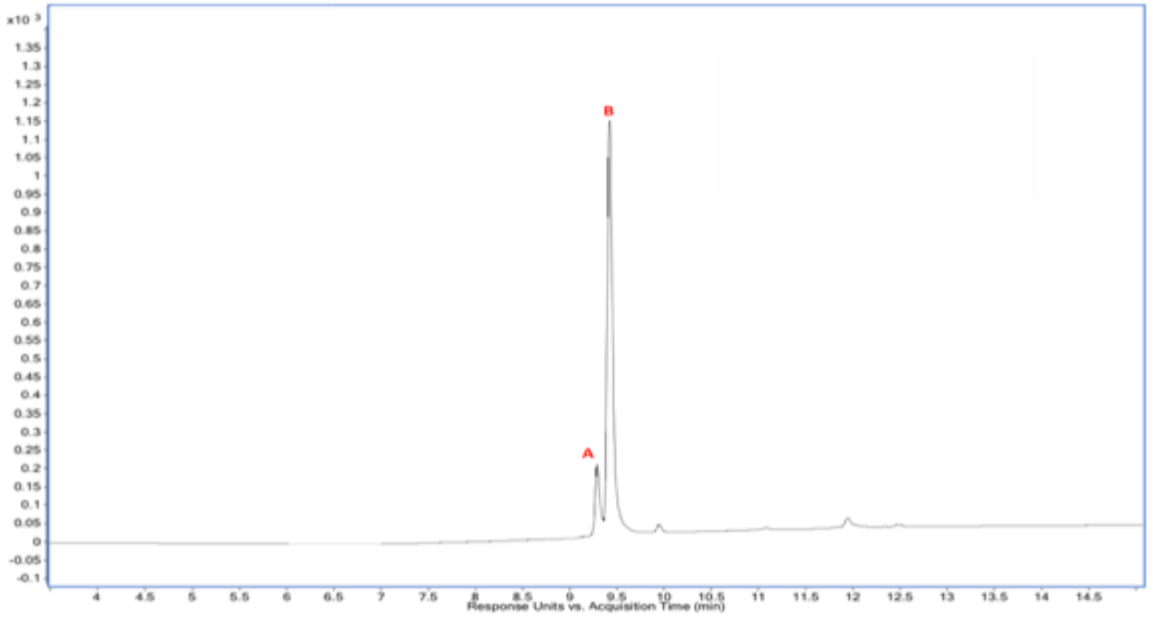


**Figure 3.9.2: Liquid chromatogram in LC-MS using ESI-TOFMS for the purified sample from the S200 elute non-tagged DM construct elution**. Trace peak A corresponds to 10374 Da and Trace B 10200 Da. Fxn A, B and C from Figure 3.8 are combined.

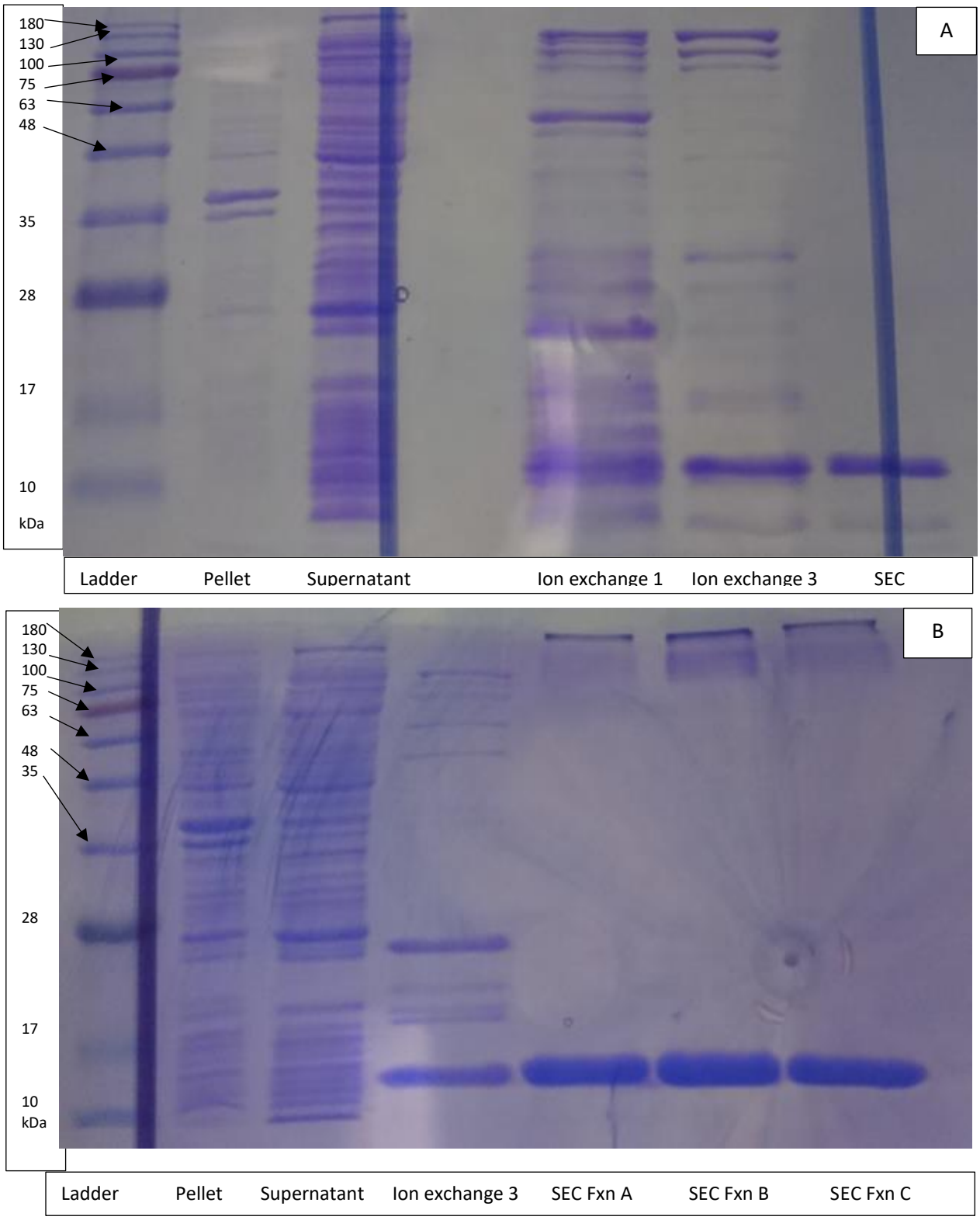


**Figure 3.10: 15% SDS-PAGE ending with S200 column purification for non-tagged constructs**. A. WT, B. DM with Fractions (Fxns) corresponding to Figure 3.8.

Results from the LC-MS suggest that purification using the S200 column does not resolve well enough for molecules of low molecular weight. Evidence can be seen from comparing the elution volume comparing WT and DM constructs. In the case of the DM, an extra peak could be seen eluting even after the whole 320 mL column void volume (**Figure 3.8**) but still contained the protein of interest upon SDS-PAGE analysis (**Figure 3.10B**). Another interesting find is that using LC-MS, two forms of the protein can be seen, one in which both clusters falls off, and the other with only one cluster attached (**Figure 3.9.2**). Other factors such as buoyancy and the overall number of charged residues on the circumference of the globular protein can cause such phenomena. Peaks B and C of the WT construct cannot be identified and require further analysis, seen in **Figure 3.9.1**. In order to solve the resolution issue, a HiPrep 26/60 S100 column was used instead of the S200 and the chromatogram is as shown below (**Figure 3.11**).

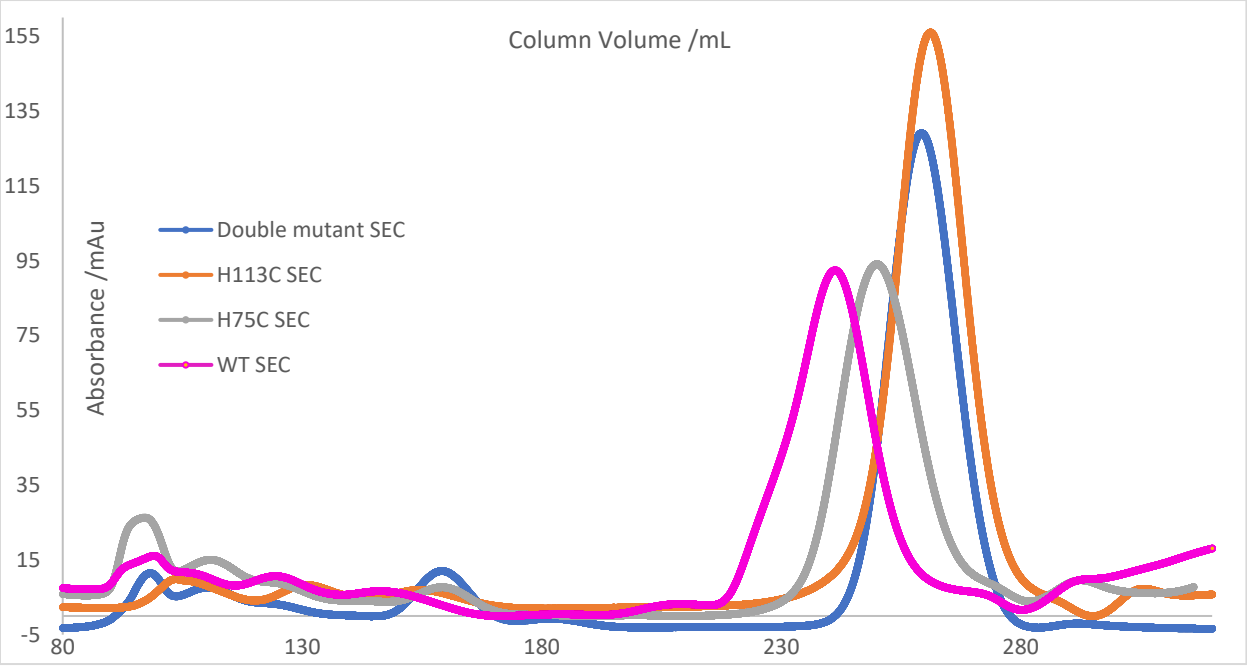


**Figure 3.11: Size exclusion chromatogram of all non-tagged MiNT constructs with an S100 size exclusion column.**

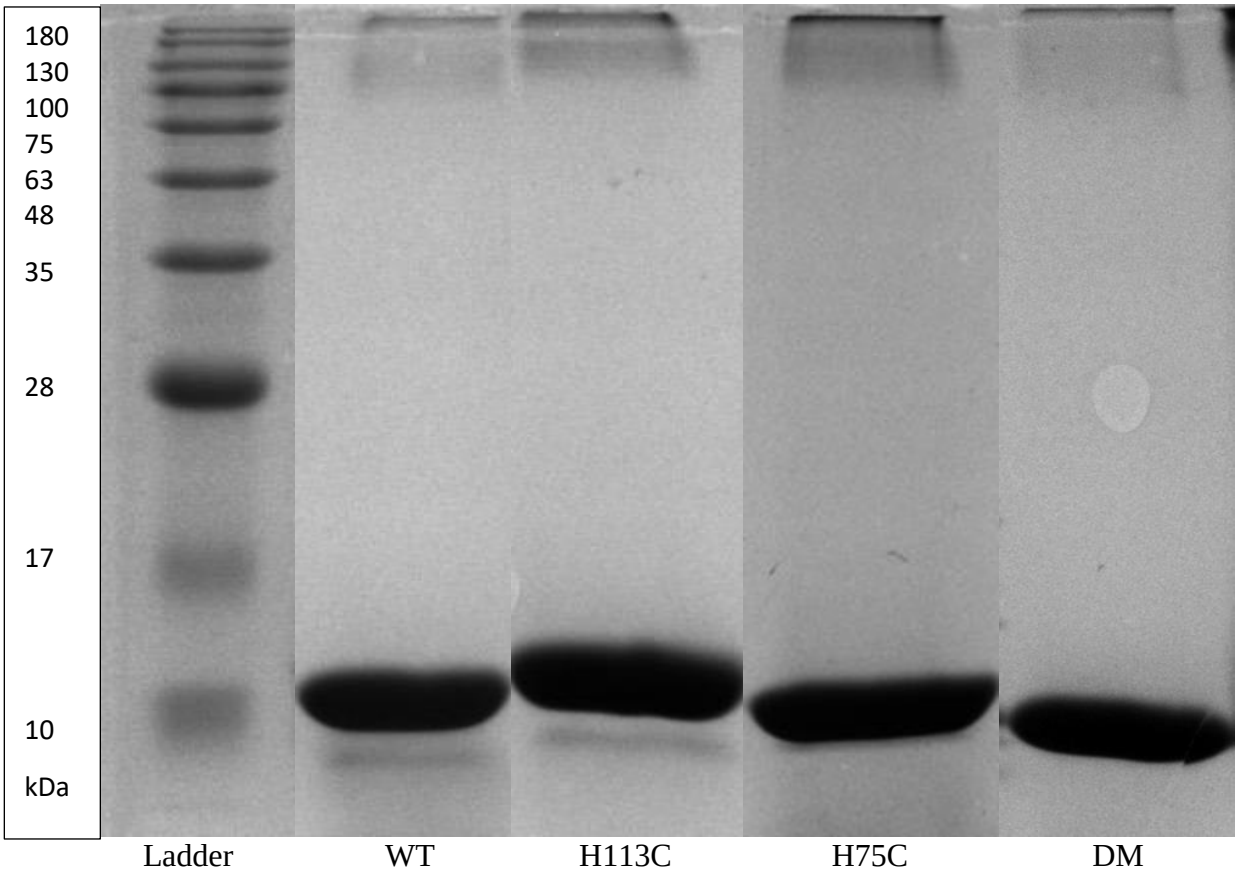


**Figure 3.12**: **15% SDS-PAGE gel for all non-tagged constructs after full purification.**

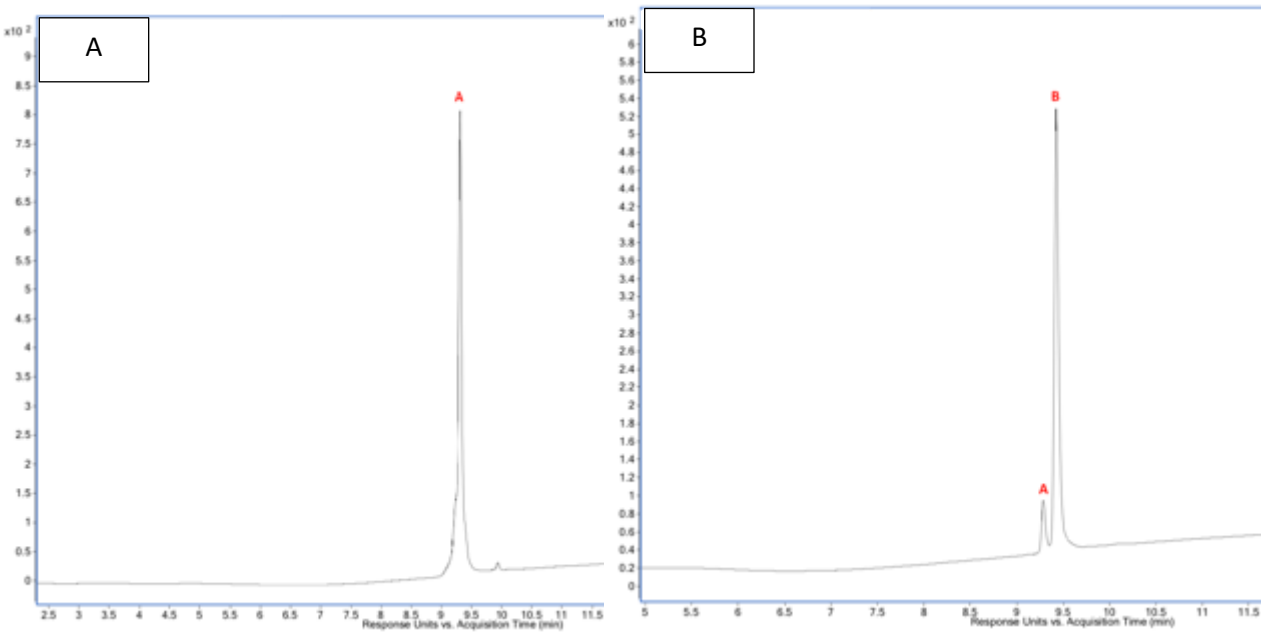


**Figure 3.13**: **Liquid chromatogram in LC-MS using ESI-TOFMS for the purified sample from S100 WT elution** (A) and DM elution (B). WT Trace peak A (A) corresponds to 10268 Da, DM Trace peak A (B) corresponds to 10375 Da and Trace peak B (B) is 10200 Da.

In conclusion, common methods like adding a His-tag does not always work well on sensitive proteins such as the MiNT. Maintaining the stability of the protein from each purification step is essential to obtain a higher yield. Troubleshooting is ultimately needed in optimize yield for the purification steps. Removal of the iron-sulfur cluster and chemical reconstitution for NEET proteins is used in purification of WT MiNT (55). However, it is not efficient as extra steps are needed to reconstitute back iron sulfur clusters, resulting in additional impurity. The purification shown above will serve as a foundation for further optimization, as the dynamics of MiNT becomes more elucidated.

# Chapter 4

## Characterization of human monomer NEET protein MiNT: Inheritance of both clusters in a single polypeptide and consequence on its properties.

## Introduction

Human cells harbor three CISD proteins that contain CDGSH iron sulfur domains; mitoNEET (mNT/CISD1), nutrient-deprivation autophagy factor 1 (NAF-1/Miner1/CISD2) and mitochondria inner NEET protein (MiNT/ Miner2/CISD3) (46, 66). Though the MiNT is similar to their homolog mNT and NAF-1, having both beta cap domain and cluster binding domains, it is a monomeric protein as opposed to a homodimeric protein (48). Sequence analysis that the cluster binding domain nearer to the N-terminus (CBD1) is flanked by several aromatic groups, unlike the environment of the cluster binding domain closer to the C-terminus (CBD2) where it contains only one tyrosine. MiNT can be found in the mitochondrial matrix and plays a role in several human cancer cells depicted in its high expressions (48, 52). Though MiNT, like other NEET proteins, is known to have redox sensor properties, in general very little is known about the specific biophysical characteristics of this protein (67). Since both CBDs harbor two 2Fe-2S clusters in different conditions, investigating MiNT's structural properties might prove further insight. In Chapter 2 and Chapter 3, the types of constructs and the purification techniques of MiNT are discussed. Biophysical assays are needed in order to accurately categorize and interpret the properties of MiNT. This is done first by mutating the histidine ligand to a cysteine ligand in each of the two positions, individually at residue number 75 and 113, as well as both positions. This chapter will describe two assays, an UV-Vis spectroscopy assay and CD assay. Here, we hypothesize that MiNT contains an electron transfer reaction system by comparing the differences between an oxidized and the reduced MiNT and its CBD1 and CBD2 mutants. We believe a certain amino acid side chain that is found in between the two CBDs of MiNT allows greater enablement in this phenomenon. Future experiments aimed at resolving this phenomenon will also be described in this chapter.

**Results and discussion**

At this time, the only available crystal structure of MiNT is the double mutant construct (PDB no: 6AVJ). This crystal structure is used as a reference for further understanding of WT MiNT in a reversed fashion. First, stability assays using UV-Vis is done at 25 °C and 37 °C respectively for all constructs to show how each cysteine mutant construct affects the overall stability of MiNT as shown below (**Figure 4.1 and Figure 4.2**).

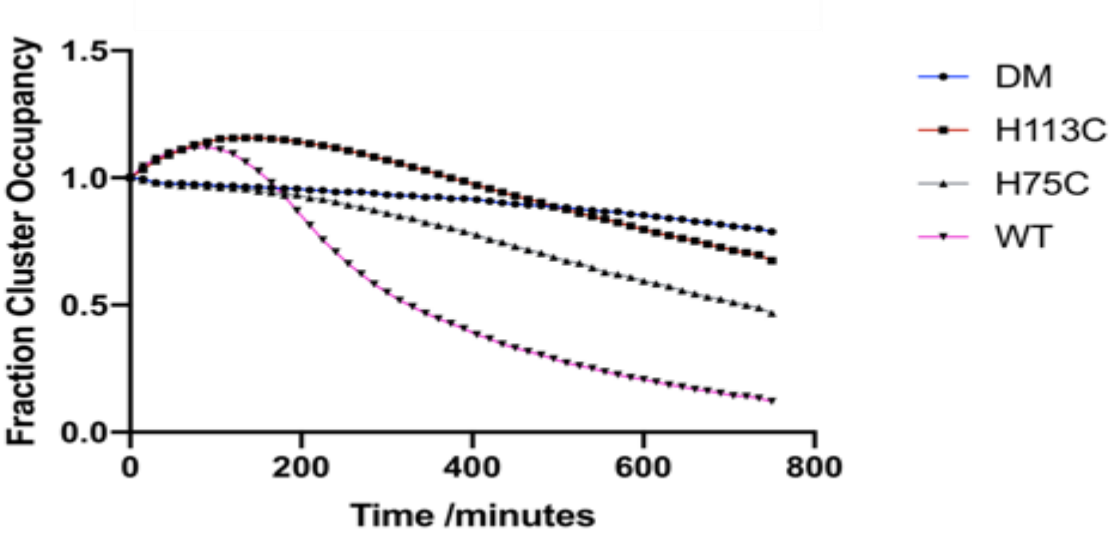


**Figure 4.1: Stability of the iron-sulfur clusters for all constructs of MiNT with time at 25 °C using 458 nm peak for each scan**. Buffer conditions are 50 mM Tris pH 8.0 and 150 mM NaCl with 20 μM of each protein construct.

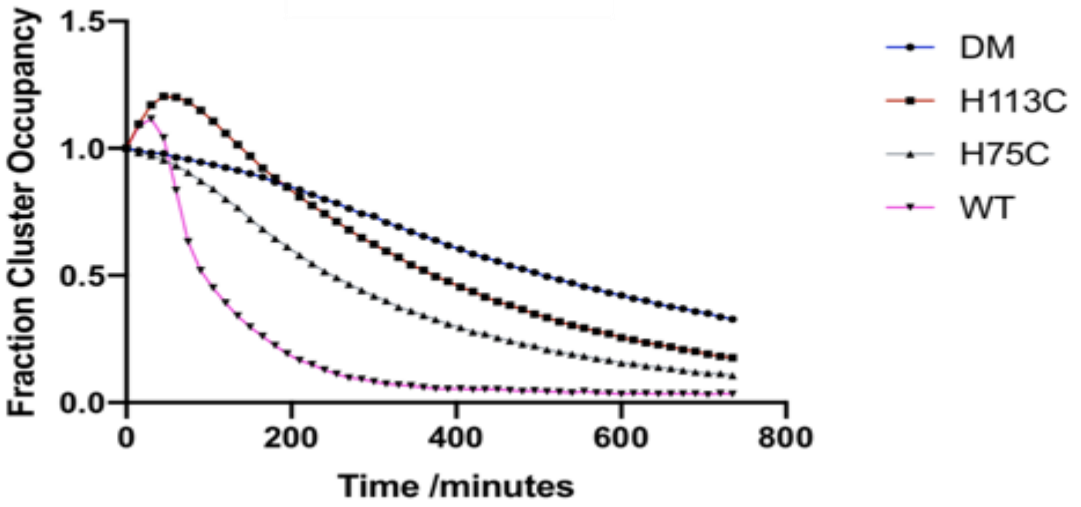


**Figure 4.2: Stability of the iron-sulfur clusters for all constructs of MiNT with time at 37 °C using 458 nm peak for each scan**. Buffer conditions are 50 mM Tris pH 8.0 and 150 mM NaCl with 20 μM of each protein construct.

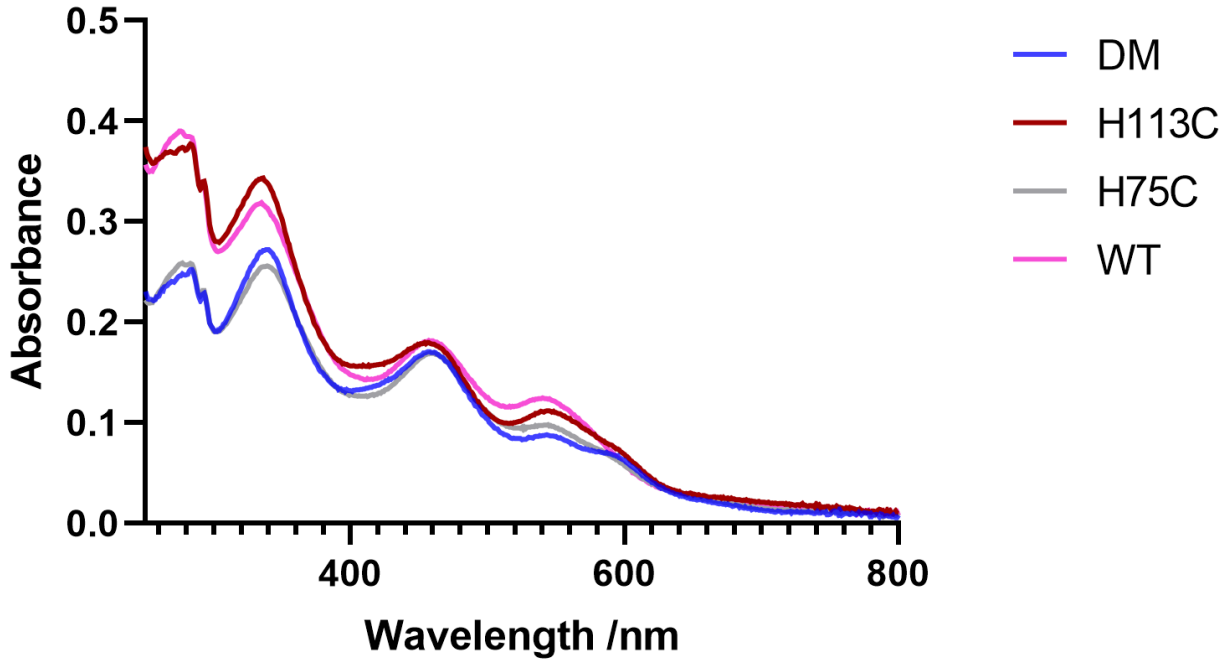


**Figure 4.3**: **Absorption scan between 250 to 800 nm wavelength of MiNT and its mutants.** Buffer conditions are 50 mM Tris pH 8.0 and 150 mM NaCl and concentration of 20 μM for each construct.

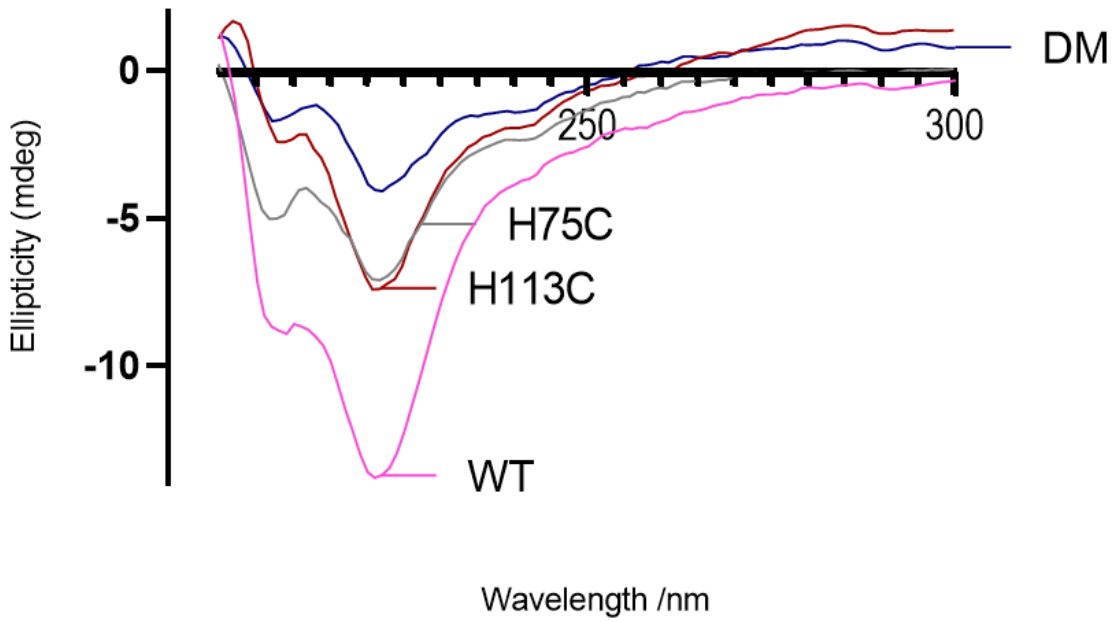


**Figure 4.4**: **Circular dichroism spectra of MiNT and its mutants scanned in a range of 200 nm to 300 nm at 15 °C.** Buffer conditions in 50 mM Tris pH 8.0 and 150 mM NaCl with 30 μM of each protein construct using 0.1 cm pathlength cuvette.

The half-life drops from ~ 330 min at 25 °C to ~ 95 minutes at 37 °C for WT MiNT, showing a dependency on temperature for overall protein stability. A similar occurrence can also be seen for the other mutant constructs of MiNT where the DM construct is the most stable, having a half-life of about 700 minutes at 37 °C. Mutation of histidine ligand to a cysteine ligand generally stabilizes the cluster due to the C2 symmetry present on the immediate ligand environment. This can also be attributed to the fact that mutation of histidine to cysteine ligand in mNT and NAF-1 result in a 6-fold and 25-fold stability increase respectively over a range of pH conditions (58, 66). An estimated stability increase of 7-fold can be seen when both ligands at position 75 and 113 of MiNT are replaced with cysteine ligands in both 25 °C and 37 °C conditions. A typical half-life of

WT mNT and WT NAF-1 is ≥ 10,000 minutes and ≥ 1000 minutes respectively while WT MiNT has a half-life of 95 minutes in pH 8.0 (40). An average of 3.6 residues per turn are needed to stabilize a carbonyl group of one amino acid and the amino group of the amino acid four residues further by hydrogen bond, thus forming an alpha helix (68). CD assay between 200 nm and 300 nm shows that the WT MiNT construct possess a more helical structure if ligands contain a histidine rather than a cysteine (**Figure 4.4**). A single mutation from histidine to cysteine at either position 75 or 113 in MiNT results in a loss in a single, complete alpha helix that can be depicted by similar ellipticity at 220 nm. It can also be understood that mutating both positions to cysteine ligand will result in a loss of both alpha helices.

Concentrations of the MiNT constructs are usually calculated by using the 458 nm peak instead of the 280 nm peak as a single 2Fe-2S ligand extinction coefficient for NEET protein is about 5000 $M^{-1}$ $cm^{-1}$ using *Arabidopsis* NEET protein as a reference (69). This has proven to be accurate for all concentration checks in regards to NEET protein due to similar environment of 3 Cys-1 His ligand. The difference between the initial peaks of the constructs in UV-Vis scanned between 200 nm and 800 nm can be seen in **Figure 4.3**. The 458 nm peak is referenced in order to gauge the stability of the clusters while they are oxidized in the case of MiNT. At the same time, it also allows for the concentration determination of holo-MiNT proteins. A deduction can be based on the difference of spectra in the 280 nm region of all MiNT constructs. H75C and DM MiNT constructs appear to have the same absorbance even though the cluster concentration is the same as the other two constructs, H113C and WT MiNT. At 280 nm, chromophores like tryptophan are major contributors of the absorbance signal, though tyrosine and possible disulfide bonds can also contribute (70). Absorbance level shows that a mutation at position 75 generally changes the environment of the position of tryptophan particularly since the sequence of MiNT indicates that

tryptophan is position right before the ligand in position 58, right before the C-X-C sequence. The UV-Vis stability assay shows that there is possible communications between clusters at position 75 while they are left in the 3 Cys-1 His environment. This is shown by the initial increase in fraction cluster occupancy in both WT and H113C MiNT constructs in both cases at 25 °C and 37 °C UV-Vis assays. A histidine ligand changed to a cysteine ligand might also dampen the signal of tryptophan by disrupting the alpha helix at position 75. Having a histidine at position 75 will allow more flexibility on the nearby residues due to a spring mechanism (71). Although additional stability of the iron-sulfur cluster can be achieved by creating a symmetrical environment with a 4-Cys ligand as shown in the stability differences, it will simultaneously limit any additional dynamics that is required for potential intermolecular crosstalk. Results show that the iron sulfur cluster at position 113 controls the overall stability of MiNT and may also indicate which order cluster transfer towards other acceptor proteins will initially occur. Human mitochondria possesses two types of ferredoxins in the mitochondrial matrix, being FDX1 and FDX2 (72). Human apo-FDXs are commonly used as iron sulfur cluster acceptors with human NEET proteins, to demonstrate and categorize cluster transfer (62, 73). In MiNT specifically, histidine ligand mutation in both positions will result in impeding its cluster transfer ability (48).

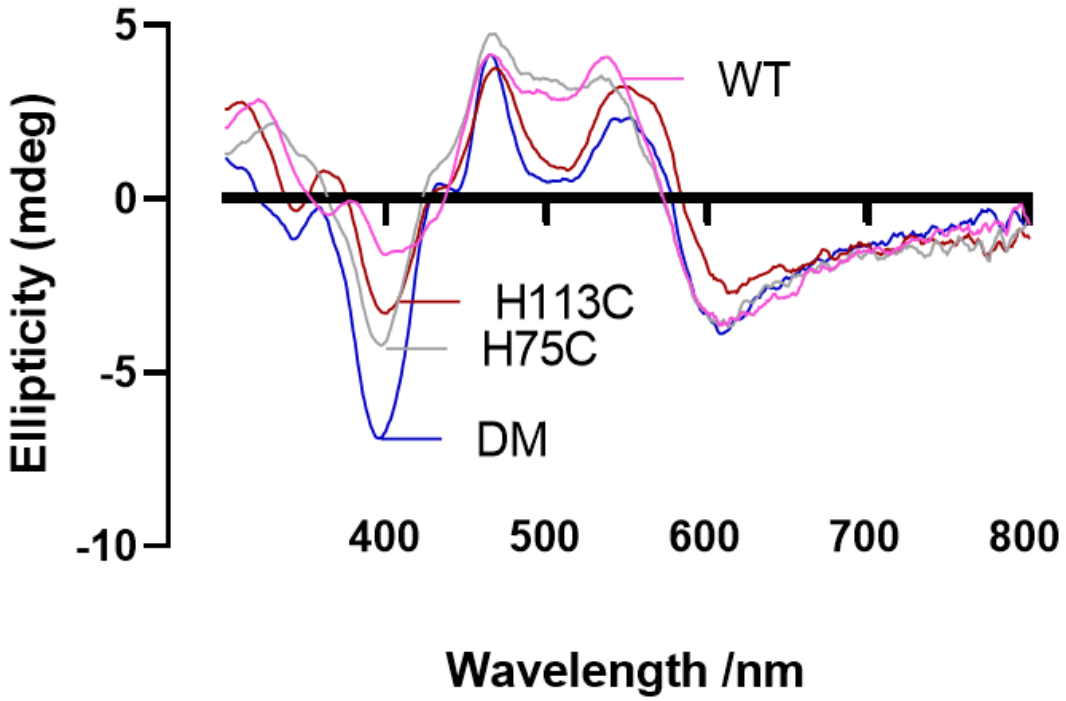


**Figure 4.5**: **Circular dichroism spectra of MiNT and its mutants scanned in a range of 300 nm to 800 nm at 15 °C**. Buffer conditions in 50 mM Tris pH 8.0 and 150 mM NaCl with 30 μM of each protein construct using 1 cm pathlength cuvette.

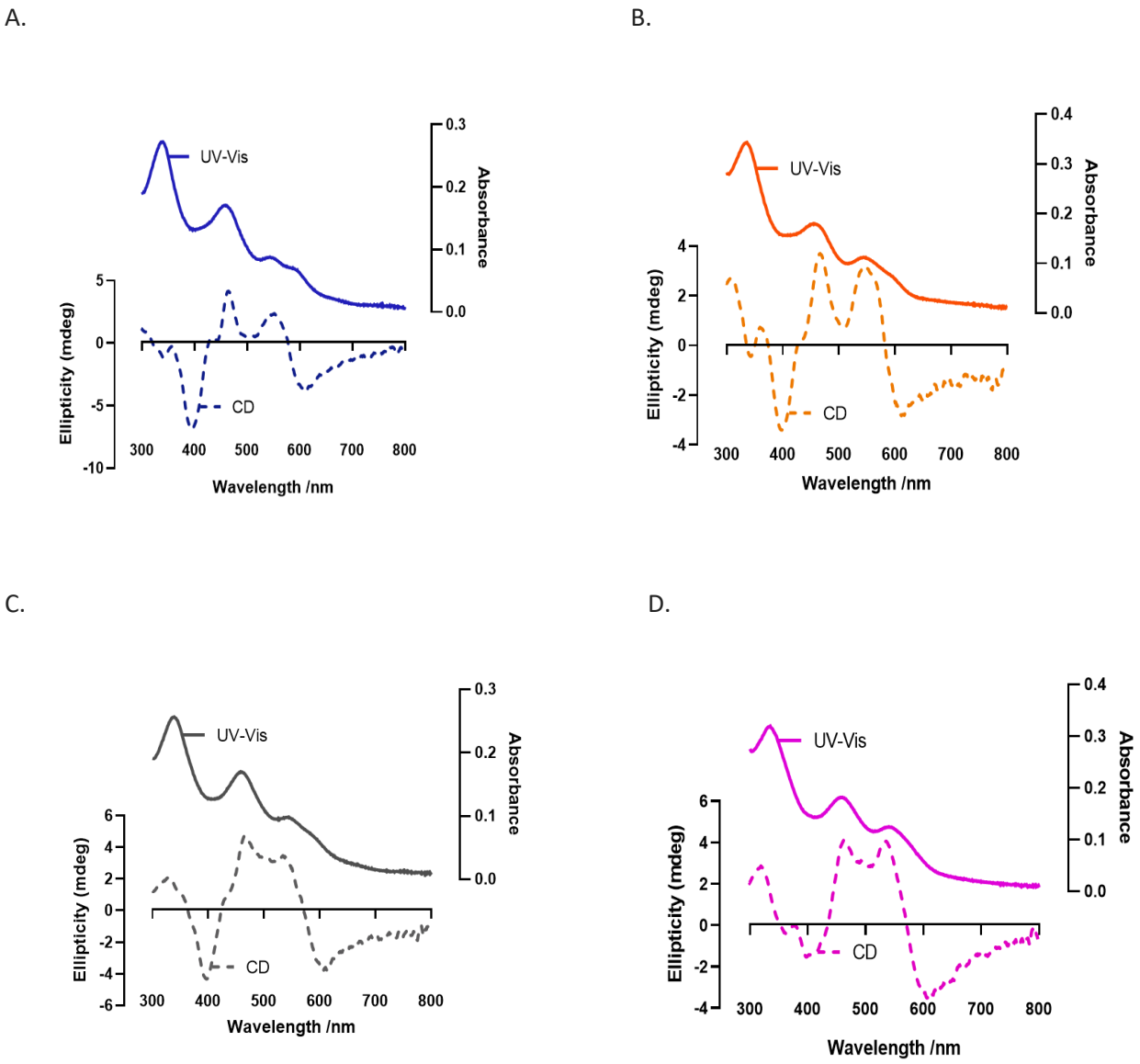


**Figure 4.6**: **Comparison spectra between UV-Vis (bold line) and circular dichroism (dotted line) assay for all MiNT constructs**. A: DM, B: H113C, C: H75C, D: WT.

Even though iron sulfur clusters are typically recognized at 458 nm in NEET proteins, peaks at around 550 nm shifts have to be considered. Stability of the cluster can also be attributed to MiNT by the shift of WT at 545 nm to 548 nm in DM MiNT construct. This shift can also be seen in H87C in mNT with additional troughs at 400 nm in CD spectra, similar to MiNT constructs in the visible range of CD (**Figure 4.5**) (58). Bathochromic effect (longer wavelength resulting in lower energy) as a result of mutation of histidine to cysteine ligand shows a change in energetics, typically for the cluster in position 113. Coupled with the stability assay results and the absorbance shift from 545 nm due to the H113C mutation, it can be shown again that CBD2 can control the overall MiNT stability. In all the WT MiNT and its mutant constructs, the absorbance peak at 458 nm remains similar, but with a slight shift in wavelength absorbance in both the UV-Vis and CD spectra.

To determine the NEET protein redox sensor characteristics, a reducing agent is usually used to determine its cluster redox potential from $[2Fe\text{-}2S]^{2+}$ to $[2Fe\text{-}2S]^{+}$ as part of an electron carrier process. Protein film voltammetry (PFV) or electron paramagnetic resonance (EPR) are mainly used to calculate the redox potential of NEET proteins (67, 74). Due to both $Fe^{3+}$ in a single cluster having a spin S = 5/2 each at positions that are exactly opposite of each other, EPR signals are silent when NEET proteins are oxidized. Thus, NEET proteins has to attain a $Fe^{2+}$ ion in a cluster through reduction to produce a signal in EPR by reduction (75, 76). Unique to NEET proteins, a potentiometric redox titration technique can also be performed using the UV-Vis spectroscopy to determine the redox potential as a blue shift could be observed while reducing agents are added to the protein sample (77). In order to understand MiNT deeper, DTT is used as a reducing agent for reduction to visualize the amount of time to achieve a fully reduced cluster by looking at the shifts over time. Since stability of MiNT is much lower compared to mNT and

NAF-1, a lower temperature of 15 °C is used for this assay. This also allows more stability during the use of DTT, thus extending the observable half-life (78). Results are as shown below in **Figure 4.7.**

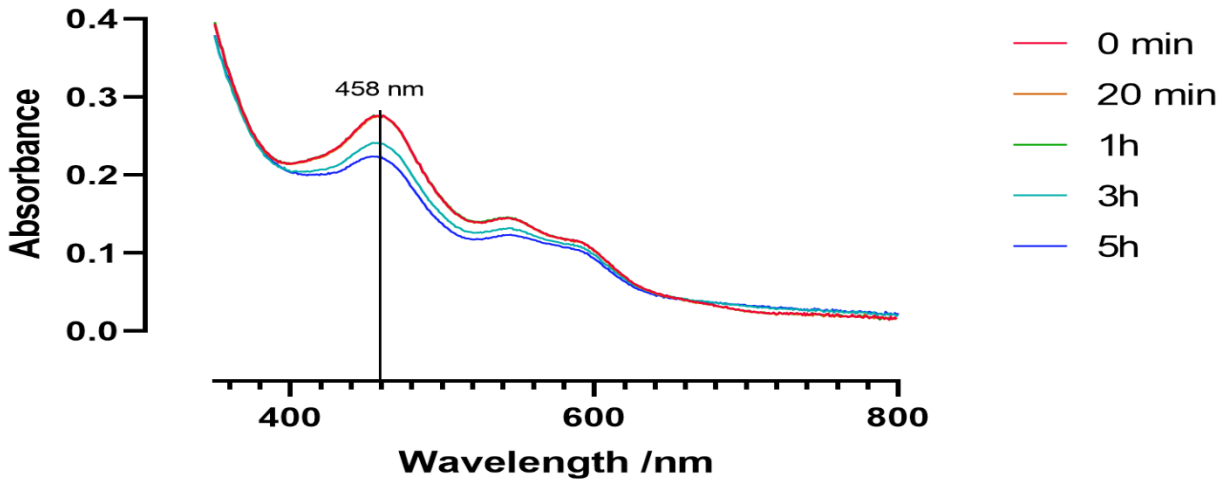


**Figure 4.7.1: DM UV-Vis spectra of 30 µM protein sample with 15 mM DTT at 15 °C in 50 mM Tris pH 8.0 and 150 mM NaCl buffer.** DM construct spectra. A 458 nm line is used as a reference to view potential hypsochromic shifts when scanning samples over time.

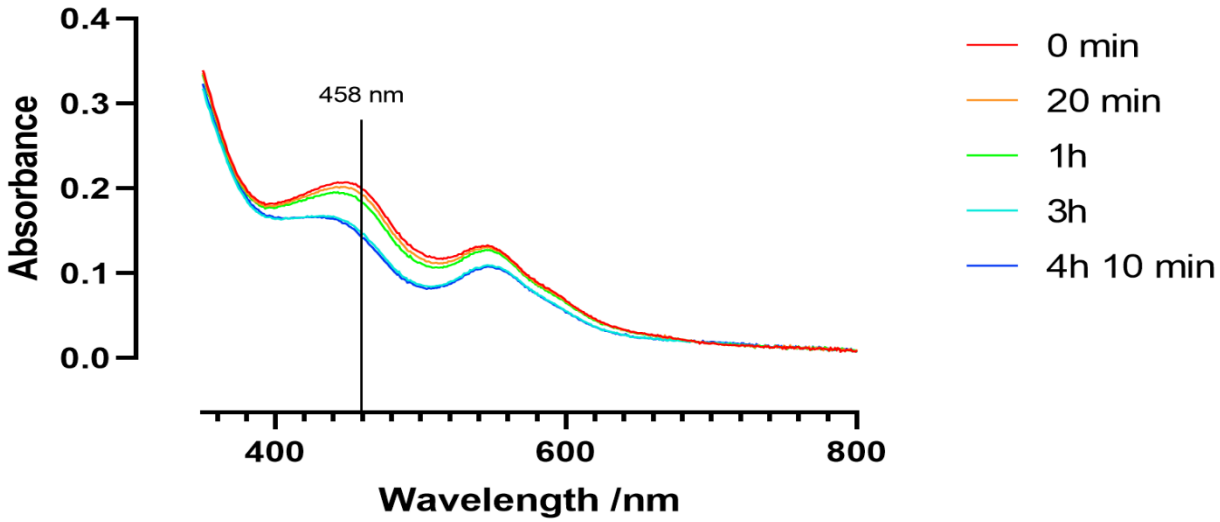


**Figure 4.7.2: H75C UV-Vis spectra of 30 µM protein sample with 15 mM DTT at 15 °C in 50 mM Tris pH 8.0 and 150 mM NaCl buffer.** H75C construct spectra. A 458 nm line is used as a reference to view potential hypsochromic shifts when scanning samples over time.

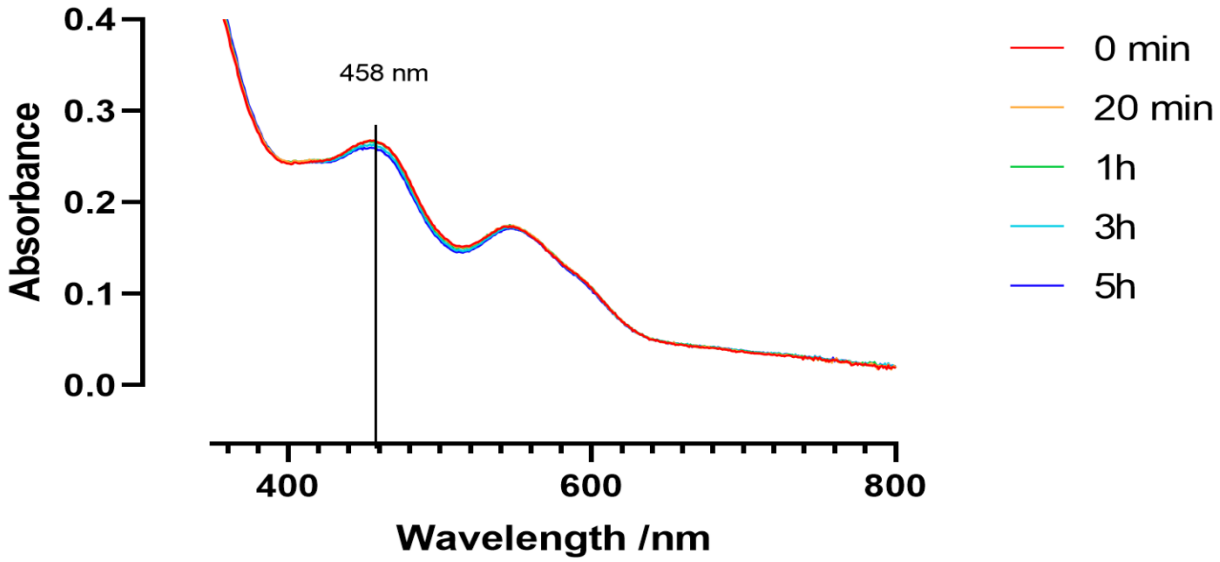


**Figure 4.7.3: H113C UV-Vis spectra of 30 µM protein sample with 15 mM DTT at 15 °C in 50 mM Tris pH 8.0 and 150 mM NaCl buffer.** H113C construct spectra. A 458 nm line is used as a reference to view potential hypsochromic shifts when scanning samples over time.

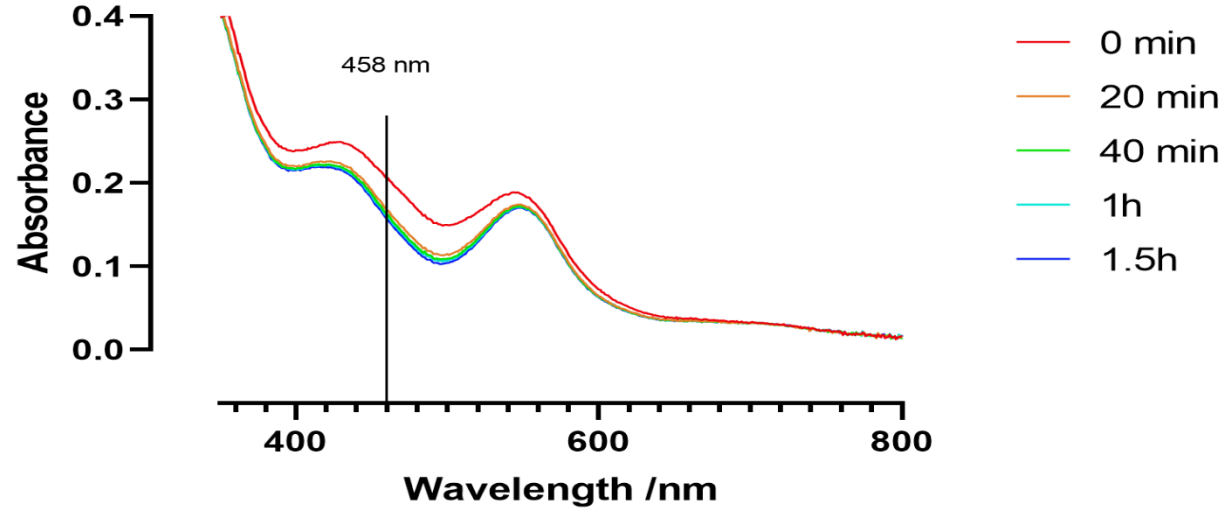


**Figure 4.7.4: WT UV-Vis spectra of 30 µM protein sample with 15 mM DTT at 15 °C in 50 mM Tris pH 8.0 and 150 mM NaCl buffer.** WT construct spectra. A 458 nm line is used as a reference to view potential hypsochromic shifts when scanning samples over time.

NEET protein clusters are typically in a reduced state in physiological conditions (79, 80). A reduced NEET protein is more stable and serves as a self- protection mechanism since cysteine ligands can be a potential target for ROS which cause modification and cleavage of protein (81). This can be seen in the slower rate of decay apart from temperature differences. From **Figure 4.7**, WT MiNT takes the least amount of time to be fully reduced at around 425 nm, which is similar to a reduced mNT spectra in UV-Vis (58, 63). We initially expected the other mutant construct to have a similar shift over time, but that is not the case (58). In H75C, the maximum blue shift ends up at around 445 nm after 4 hours of exposure to DTT. For both DM and H113C constructs, there are virtually no shifts even with a considerable concentration difference between the protein samples and the DTT added. The redox potential of DTT is around -370 mV at pH 8.1 and oxidized DTT has a peak around 280 nm that stretches across wavelength up to 340 nm due to the formation of indole ring while oxidized (82, 83). 2Fe-2S cluster centers can possess a wide range of redox potentials for different proteins, with the ability to be engineered for a wider range in different pH conditions (77, 84). Based on the shifts shown in the UV-Vis spectra in all reduced MiNT constructs, CBD2 dictates the protein electron acceptor properties. This is expected because the aromatic groups surrounding CBD1 in MiNT may not allow the entrance of DTT for cluster to be reduced. This explains why the shift does not go as expected to around 425 nm in the mutant constructs of MiNT as opposed to similar ligand environment in both mNT and NAF-1. The shift to 445 nm in H75C construct indicates that only CBD2 cluster is reduced while CBD1 cluster is still oxidized. Results from H113C and DM constructs point out that if the cluster in CBD2 is not reduced, both the clusters will not be reduced, thus produces no shift in the 458 nm wavelength. Referring back to **Figure 4.3**, immediate ligand environment at CBD1 is the same by having the same extinction coefficients at 280 nm in WT and H113C constructs as opposed to the other two

mutant constructs. This phenomenon differentiates the MiNT's properties from that of mNT and NAF-1.

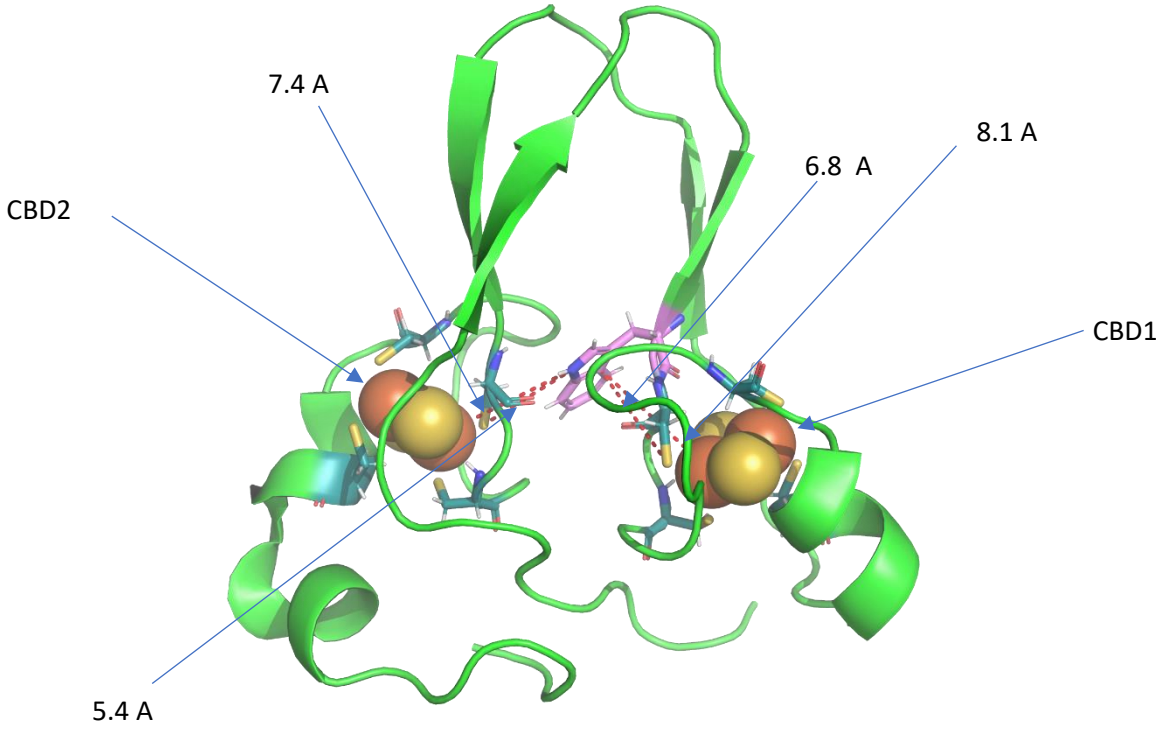


**Figure 4.8**: **Crystal structure of DM MiNT construct continued.** The crystal structure of DM MiNT (PDB no: 6AVJ) with cysteine residues denoted by cyan and tryptophan residue 76 in magenta. Both CBDs is denoted with arrows and possible electron transfer network, via tryptophan, is indicated by red dotted lines. Yellow and blue sticks indicate thiol groups and nitrogen atoms, and orange spheres indicate iron ion.

Biological redox enzymes containing metal centers such as cytochrome *c* peroxidase and ribonucleotide reductase each contain a long-range charge transport system (85, 86). Aromatic side chains such as tryptophan or tyrosine are able to accommodate electron hopping by providing a stable intermediate (87, 88). Azurin, a blue copper protein is used as a classic model for studying tryptophan radicals (89). However, in MiNT, as shown in **Figure 4.8**, we propose that the tryptophan acts as a conduit facilitating communication between the two clusters. The distance indicated for possible electron transfer show that this event is feasible as electron tunneling can happen between centers up to 20 or 30 Å, which make this residue a feasible target for investigation in electronic transition (90). Further evidences point to the role of the tryptophan interaction between the iron sulfur clusters is shown in an EPR pulse sequence in the Q-band showing weak interaction to a residue in $^{15}N$ labeled mNT (75). As mentioned, the crystal structure is a DM construct of MiNT, indicating that the loss of the two histidine ligands result in the reduction of the flexibility of the helix near each of the cluster. This means that distances between the ligands and tryptophan can be closer, increasing the probability of a role in electron transfer. Since DTT is polar, it cannot easily access through the aromatic side chains in order to reduce the cluster in CBD1, as shown in **Figure 4.7**. Therefore, a mechanism is needed in order to achieve full reduction of MiNT. Due to its asymmetry this is unique only to the monomeric MiNT as opposed to the homologous mNT and NAF-1. A mutation from a histidine to a cysteine ligand at position 113 results in a much-lowered redox potential and DTT is not able to reduce it efficiently. This suggest that there could be larger prospective range of redox potential engineering for NEET proteins much more than before by only using mNT (77). Due to the WT MiNT iron-sulfur cluster instability compared to the other two human NEET proteins, cluster loss occurs within a short interval and

as such allowing efficient electron transfer may be an integrated importance to the overall protein stability.

**Future Directions**

Even though some characteristics of MiNT have been elucidated, further investigations have to be done to get a more accurate insight into the electron communication network of MiNT. For all MiNT constructs mentioned above, the next step is to perform a point mutation on the tryptophan to another aromatic residue like phenylalanine or an equivalent homo-amino acid. This mutation should not affect the overall structure by much due to the phenylalanine residue's hydrophobicity and a presence of a bulky aromatic group, but would eliminate the role of any facilitated electron transfer reactions. We expect changes in the redox potential if tryptophan facilitates communication. pH dependent EPR or UV-Vis redox titration can be performed for the WT MiNT in order to further understand its redox potential range in varying pH. Raman or infrared spectroscopy can also be utilized to further understand the vibrational states of the structure between MiNT constructs. Though MiNT has a role in several cancers, there are still many aspects of MiNT to be explored and the findings shown in this chapter will help illustrate further roles in the ISC pathway.

References


1. Bandyopadhyay, S.; Chandramouli, K.; Johnson, M. K. Iron-sulfur cluster biosynthesis. *Biochem Soc Trans*. **2008,** *36 (pt6)*, 1112-1119.

2. Johnson, D. C.; Dean, D. R.; Smith, A. D.; Johnson, M. K. STRUCTURE, FUNCTION, AND FORMATION OF BIOLOGICAL IRON-SULFUR CLUSTERS. *Annu Rev Biochem.* **2005,** *74*, 247-281.

3. Ayala-Castro, C.; Saini, A.; Outten, F. W. Fe-S cluster assembly pathways in bacteria. *Microbiol Mol Biol Rev.* **2008,** *72 (1)*, 110-125.

4. Wächtershäuser, G. Groundworks for an evolutionary biochemistry: The iron-sulphur world. *Prog Biophys Mol Biol.* **1992,** *58 (2)*, 85-201.

5. Fontecave, M. Iron-sulfur clusters: ever-expanding roles. *Nat Chem Biol.* **2006,** *2 (4)*, 171-174.

6. Barras, F. Iron–Sulfur Proteins: Structure, Function and Biogenesis. *eLS.* **2017,** 1-9.

7. Beinert, H.; Holm, R. H.; Münck, E. Iron-Sulfur Clusters: Nature's Modular, Multipurpose Structures. *Science.* **1997,** *277 (5326)*, 653-659.

8. Nakamaru-Ogiso‡, E.; Yano, T.; Ohnishi, T. Characterization of the Iron-Sulfur Cluster Coordinated by a Cysteine Cluster Motif (CXXCXXXCX27C) in the Nqo3 Subunit in the Proton-translocating NADH-Quinone Oxidoreductase (NDH-1) of Thermus thermophilus HB-8*. *J Biol Chem.* **2002,** *277 (3)*, 1680-1688.

9. Crack, J. C.; Green, J.; Thomson, A. J.; Le Brun, N. E. Iron-sulfur clusters as biological sensors: the chemistry of reactions with molecular oxygen and nitric oxide. *Acc Chem Res.* **2014,** *47 (10)*, 3196-3205.

10. Qi, W.; Cowan, J. A. Structural, Mechanistic and Coordination Chemistry of Relevance to the Biosynthesis of Iron-Sulfur and Related Iron Cofactors. *Coord Chem Rev.* **2011,** *255 (7-8)*, 688-699.

11. Schilke, B.; Voisine, C.; Beinert, H.; Craig, E. Evidence for a conserved system for iron metabolism in the mitochondria of Saccharomyces cerevisiae. *Proc Natl Acad Sci U S A.* **1999,** *96 (18)*, 10206-10211.

12. Gisselberg, J. E.; Dellibovi-Ragheb, T. A.; Matthews, K. A.; Bosch, G.; Prigge, S. T. The Suf Iron-Sulfur Cluster Synthesis Pathway Is Required for Apicoplast Maintenance in Malaria Parasites. *PLoS Pathog.* **2013,** *9 (9)*, e1003655.

13. Liu, Y.; Sieprawska-Lupa, M.; Whitman, W. B.; White, R. H. Cysteine is not the sulfur source for iron-sulfur cluster and methionine biosynthesis in the methanogenic archaeon Methanococcus maripaludis. *J Biol Chem*. **2010,** *285 (42)*, 31923-31929.

14. Frazzon, J.; Fick, J. R.; Dean, D. R. Biosynthesis of iron-sulphur clusters is a complex and highly conserved process. *Biochem Soc Trans.* **2002,** *30 (4)*, 680-685.

15. Stehling, O.; Lill, R. The role of mitochondria in cellular iron-sulfur protein biogenesis: mechanisms, connected processes, and diseases. *Cold Spring Harb Perspect Biol.* **2013,** *5 (8)*, a011312.

16. Sharma, A. K.; Pallesen, L. J.; Spang, R. J.; Walden, W. E. Cytosolic iron-sulfur cluster assembly (CIA) system: factors, mechanism, and relevance to cellular iron regulation. *J Biol Chem.* **2010,** *285 (35)*, 26745-26751.

17. Ciofi-Baffoni, S.; Nasta, V.; Banci, L. Protein networks in the maturation of human iron–sulfur proteins. *Metallomics.* **2018,** *10 (1), 49-72.*

18. Andreini, C.; Banci, L.; Bertini, I.; Rosato, A. Occurrence of copper proteins through the three domains of life: a bioinformatic approach. *J Proteome Res.* **2008,** *7 (1)*, 209-216.

19. Cabantchik, Z. I. Labile iron in cells and body fluids: physiology, pathology, and pharmacology. *Front Pharmacol.* **2014,** *5*, 45.

20. Kivrak, E. G.; Yurt, K. K.; Kaplan, A. A.; Alkan, I.; Altun, G. Effects of electromagnetic fields exposure on the antioxidant defense system. *J Microsc Ultrastruct.* **2017,** *5(4)*, 167-176.

21. Kruszewski, M. The role of labile iron pool in cardiovascular diseases. *Acta Biochim Pol.* **2004,** *51 (2)*, 471-480.

22. Shah, S. V.; Rajapurkar, M. M. The role of labile iron in kidney disease and treatment with chelation. *Hemoglobin.* **2009,** *33 (5)*, 378-385.

23. Reelfs, O.; Abbate, V.; Cilibrizzi, A.; Pook, M. A.; Hider, R. C.; Pourzand, C. The role of mitochondrial labile iron in Friedreich's ataxia skin fibroblasts sensitivity to ultraviolet A. *Metallomics.* **2019,** *11 (3)*, 656-665.

24. Belaidi, A. A.; Bush, A. I. Iron neurochemistry in Alzheimer's disease and Parkinson's disease: targets for therapeutics. *J Neurochem*. **2016,** *139 Suppl 1*, 179-197.

25. Cutrin, J. C.; Alberti, D.; Bernacchioni, C.; Ciambellotti, S.; Turano, P.; Luchinat, C.; Crich, S. G.; Aime, S. Cancer cell death induced by ferritins and the peculiar role of their labile iron pool. *Oncotarget.* **2018,** *9 (46)*, 27974-27984.

26. Wachnowsky, C.; Fidai, I.; Cowan, J. A. Iron–sulfur cluster biosynthesis and trafficking – impact on human disease conditions. *Metallomics.* **2018,** *10 (1),* 9-29.

27. Braymer, J. J.; Lill, R. Iron-sulfur cluster biogenesis and trafficking in mitochondria. *J Biol Chem.* **2017,** *292 (31),* 12754-12763.

28. Vernis; Laurence; Banna, E.; Nadine; Hatem; Elie; Heneman; Amélie; Huang. Fe-S Clusters Emerging as Targets of Therapeutic Drugs. *Oxid Med Cell Longev*. **2017,** *2017*, 3647657.

29. Qi, W.; Li, J.; Cowan, J. A. Human ferredoxin-2 displays a unique conformational change. *Dalton Trans.* **2013,** *42 (9),* 3088-3091.

30. Ferraro, D. J.; Gakhar, L.; Ramaswamy, S. Rieske business: structure-function of Rieske non-heme oxygenases. *Biochem Biophys Res Commun.* **2005,** *338 (1),* 175-190.

31. Paddock, M. L.; Wiley, S. E.; Axelrod, H. L.; Cohen, A. E.; Roy, M.; Abresch, E. C.; Capraro, D.; Murphy, A. N.; Nechushtai, R.; Dixon, J. E.; Jennings, P. A. MitoNEET is a uniquely folded 2Fe 2S outer mitochondrial membrane protein stabilized by pioglitazone. *Proc Natl Acad Sci U S A.* **2007,** *104 (36),* 14342-14347.

32. Hou, X.; Liu, R.; Ross, S.; Smart, E. J.; Zhu, H.; Gong, W. Crystallographic studies of human MitoNEET. *J Biol Chem.* **2007,** *282 (46),* 33242-33246.

33. Feinstein, D. L.; Spagnolo, A.; Akar, C.; Weinberg, G.; Murphy, P.; Gavrilyuk, V.; Dello Russo, C. Receptor-independent actions of PPAR thiazolidinedione agonists: is mitochondrial function the key? *Biochem Pharmacol*. **2005,** *70(2)*, 177-188.

34. Stockl, K. M.; Le, L.; Zhang, S.; Harada, A. S. M. Risk of acute myocardial infarction in patients treated with thiazolidinediones or other antidiabetic medications. *Pharmacoepidemiol Drug Saf.* **2009,** *18 (2),* 166-174.

35. Shaya, F. T.; Lu, Z.; Sohn, K.; Weir, M. R. Thiazolidinediones and cardiovascular events in high-risk patients with type-2 diabetes mellitus: a comparison with other oral antidiabetic agents. *P T.* **2009,** *34 (9),* 490-494.

36. Pérez, M. J.; Quintanilla, R. A. Therapeutic Actions of the Thiazolidinediones in Alzheimer's Disease. *PPAR Res.* **2015,** *2015*, 957248.

37. Wu, H.-F.; Kao, L.-T.; Shih, J.-H.; Kao, H.-H.; Chou, Y.-C.; Li, I.-H.; Kao, S. Pioglitazone use and Parkinson's disease: a retrospective cohort study in Taiwan. *BMJ Open.* **2018,** *8 (8),* e023302.

38. Chang, N. C.; Nguyen, M.; Bourdon, J.; Risse, P.-A.; Martin, J.; Danialou, G.; Rizzuto, R.; Petrof, B. J.; Shore, G. C. Bcl-2-associated autophagy regulator Naf-1 required for maintenance of skeletal muscle. *Hum Mol Genet.* **2012,** *21 (10),* 2277-2287.

39. Chang, N. C.; Nguyen, M.; Germain, M.; Shore, G. C. Antagonism of Beclin 1-dependent autophagy by BCL-2 at the endoplasmic reticulum requires NAF-1. http://emboj.embopress.org/content/29/3/606.abstract (accessed May 3, 2019). *EMBO K.* **2010,** *29 (3)*, 606-618.

40. Conlan, A. R.; Axelrod, H. L.; Cohen, A. E.; Abresch, E. C.; Zuris, J.; Yee, D.; Nechushtai, R.; Jennings, P. A.; Paddock, M. L. Crystal structure of Miner1: The redox-active 2Fe-2S protein causative in Wolfram Syndrome 2. *J Mol Biol.* **2009,** *392(1)*, 143-153.

41. Maiuri, M. C.; Criollo, A.; Kroemer, G. Crosstalk between apoptosis and autophagy within the Beclin 1 interactome. *EMBO J.* **2010,** *29 (3)*, 515-516.

42. Amr, S.; Heisey, C.; Zhang, M.; Xia, X.-J.; Shows, K. H.; Ajlouni, K.; Pandya, A.; Satin, L. S.; El-Shanti, H.; Shiang, R. A homozygous mutation in a novel zinc-finger protein, ERIS, is responsible for Wolfram syndrome 2. *Am J Hum Genet.* **2007,** *81 (4)*, 673-683.

43. Wolfram syndrome - Genetics Home Reference - NIH. https://ghr.nlm.nih.gov/condition/wolfram-syndrome (accessed May 3, 2019).

44. Sohn, Y.-S.; Tamir, S.; Song, L.; Michaeli, D.; Matouk, I.; Conlan, A. R.; Harir, Y.; Holt, S. H.; Shulaev, V.; Paddock, M. L.; Hochberg, A.; Cabanchick, I. Z.; Onuchic, J. N.; Jennings, P. A.; Nechushtai, R.; Mittler, R. NAF-1 and mitoNEET are central to human breast cancer proliferation by maintaining mitochondrial homeostasis and promoting tumor growth. *Proc Natl Acad Sci U S A.* **2013,** *110 (36)*, 14676-14681.

45. Chen, Y.-F.; Kao, C.-H.; Chen, Y.-T.; Wang, C.-H.; Wu, C.-Y.; Tsai, C.-Y.; Liu, F.-C.; Yang, C.-W.; Wei, Y.-H.; Hsu, M.-T.; Tsai, S.-F.; Tsai, T.-F. Cisd2 deficiency drives premature aging and causes mitochondria-mediated defects in mice. *Genes Dev.* **2009,** *23 (10)*, 1183-1194.

46. Wiley, S. E.; Murphy, A. N.; Ross, S. A.; van der Geer, P.; Dixon, J. E. MitoNEET is an iron-containing outer mitochondrial membrane protein that regulates oxidative capacity. *Proc Natl Acad Sci U S A.* **2007,** *104 (13)*, 5318-5323.

47. Conlan, A. R.; Paddock, M. L.; Axelrod, H. L.; Cohen, A. E.; Abresch, E. C.; Wiley, S.; Roy, M.; Nechushtai, R.; Jennings, P. A. The novel 2Fe-2S outer mitochondrial protein mitoNEET displays conformational flexibility in its N-terminal cytoplasmic tethering domain. *Acta Crystallogr Sect F Struct Biol Cryst Commun.* **2009,** *65 (pt7)*, 654-659.

48. Lipper, C. H.; Karmi, O.; Sohn, Y. S.; Darash-Yahana, M.; Lammert, H.; Song, L.; Liu, A.; Mittler, R.; Nechushtai, R.; Onuchic, J. N.; Jennings, P. A. Structure of the human monomeric NEET protein MiNT and its role in regulating iron and reactive oxygen species in cancer cells. *Proc Natl Acad Sci U S A.* **2018,** *115 (2)*, 272-277.

49. Karmi, O.; Marjault, H.-B.; Pesce, L.; Carloni, P.; Onuchic, J. N.; Jennings, P. A.; Mittler, R.; Nechushtai, R. The unique fold and lability of the [2Fe-2S] clusters of NEET proteins

mediate their key functions in health and disease. *J Biol Inorg Chem*. **2018,** *23 (4)*, 599-612.

50. Lin, J.; Zhang, L.; Lai, S.; Ye, K. Structure and molecular evolution of CDGSH iron-sulfur domains. *PLoS One.* **2011,** *6(9)*, e24790.

51. Sengupta, S.; Nechushtai, R.; Jennings, P. A.; Onuchic, J. N.; Padilla, P. A.; Azad, R. K.; Mittler, R. Phylogenetic analysis of the CDGSH iron-sulfur binding domain reveals its ancient origin. *Sci Rep.* **2018,** *8 (1)*, 4840.

52. Expression of CISD3 in cancer - Summary - The Human Protein Atlas. https://www.proteinatlas.org/ENSG00000277972-CISD3/pathology (accessed May 3, 2019).

53. Wain, L. V.; Shrine, N.; Artigas, M. S.; Erzurumluoglu, A. M.; Noyvert, B.; Bossini-Castillo, L.; Obeidat, M.; Henry, A. P.; Portelli, M. A.; Hall, R. J.; Billington, C. K.; Rimington, T. L.; Fenech, A. G.; John, C.; Blake, T.; Jackson, V. E.; Allen, R. J.; Prins, B. P.; Understanding Society Scientific Group; Campbell, A.; Porteous, D. J.; Jarvelin, M.-R.; Wielscher, M.; James, A. L.; Hui, J.; Wareham, N. J.; Zhao, J. H.; Wilson, J. F.; Joshi, P. K.; Stubbe, B.; Rawal, R.; Schulz, H.; Imboden, M.; Probst-Hensch, N. M.; Karrasch, S.; Gieger, C.; Deary, I. J.; Harris, S. E.; Marten, J.; Rudan, I.; Enroth, S.; Gyllensten, U.; Kerr, S. M.; Polasek, O.; Kähönen, M.; Surakka, I.; Vitart, V.; Hayward, C.; Lehtimäki, T.; Raitakari, O. T.; Evans, D. M.; Henderson, A. J.; Pennell, C. E.; Wang, C. A.; Sly, P. D.; Wan, E. S.; Busch, R.; Hobbs, B. D.; Litonjua, A. A.; Sparrow, D. W.; Gulsvik, A.; Bakke, P. S.; Crapo, J. D.; Beaty, T. H.; Hansel, N. N.; Mathias, R. A.; Ruczinski, I.; Barnes, K. C.; Bossé, Y.; Joubert, P.; van den Berge, M.; Brandsma, C.-A.; Paré, P. D.; Sin, D. D.; Nickle, D. C.; Hao, K.; Gottesman, O.; Dewey, F. E.; Bruse, S. E.; Carey, D. J.; Kirchner, H. L.; Geisinger-Regeneron DiscovEHR Collaboration; Jonsson, S.; Thorleifsson, G.; Jonsdottir, I.; Gislason, T.; Stefansson, K.; Schurmann, C.; Nadkarni, G.; Bottinger, E. P.; Loos, R. J. F.; Walters, R. G.; Chen, Z.; Millwood, I. Y.; Vaucher, J.; Kurmi, O. P.; Li, L.; Hansell, A. L.; Brightling, C.; Zeggini, E.; Cho, M. H.; Silverman, E. K.; Sayers, I.; Trynka, G.; Morris, A. P.; Strachan, D. P.; Hall, I. P.; Tobin, M. D. Genome-wide association analyses for lung function and chronic obstructive pulmonary disease identify new loci and potential druggable targets. *Nat Genet.* **2017,** *49 (3)*, 416-425.

54. Chronic obstructive pulmonary disease (COPD). https://www.who.int/news-room/fact-sheets/detail/chronic-obstructive-pulmonary-disease-(copd) (accessed May 3, 2019).

55. Cheng, Z.; Landry, A. P.; Wang, Y.; Ding, H. Binding of Nitric Oxide in CDGSH-type [2Fe-2S] Clusters of the Human Mitochondrial Protein Miner2. *J Biol Chem*. **2017,** *292 (8)*, 3146-3153.

56. Duan, X.; Yang, J.; Ren, B.; Tan, G.; Ding, H. Reactivity of nitric oxide with the [4Fe-4S] cluster of dihydroxyacid dehydratase from Escherichia coli. *Biochem J.* **2009,** *417 (3)*, 783-789.

57. Rogers, P. A.; Ding, H. L-cysteine-mediated destabilization of dinitrosyl iron complexes in proteins. *J Biol Chem.* **2001,** *276 (33)*, 30980-30986.

58. Conlan, A. R.; Paddock, M. L.; Homer, C.; Axelrod, H. L.; Cohen, A. E.; Abresch, E. C.; Zuris, J. A.; Nechushtai, R.; Jennings, P. A. Mutation of the His ligand in mitoNEET stabilizes the 2Fe-2S cluster despite conformational heterogeneity in the ligand environment. *Acta Crystallogr D Biol Crystallogr.* **2011,** *67 (pt 6)*, 516-523.

59. PureLink Quick Plasmid Miniprep Kits - 2013.igem.org. http://2013.igem.org/wiki/images/e/ed/BGU_purelink_quick_plasmid_qrc.pdf (accessed May 3, 2019).

60. Booth, W. T.; Schlachter, C. R.; Pote, S.; Ussin, N.; Mank, N. J.; Klapper, V.; Offermann, L. R.; Tang, C.; Hurlburt, B. K.; Chruszcz, M. Impact of an N-terminal Polyhistidine Tag on Protein Thermal Stability. *ACS Omega.* **2018,** *3 (1)*, 760-768.

61. Uhlén, M.; Forsberg, G.; Moks, T.; Hartmanis, M.; Nilsson, B. Fusion proteins in biotechnology. *Curr Opin Biotechnol.* **1992,** *3 (4)*, 363-369.

62. Tamir, S.; Eisenberg-Domovich, Y.; Conlan, A. R.; Stofleth, J. T.; Lipper, C. H.; Paddock, M. L.; Mittler, R.; Jennings, P. A.; Livnah, O.; Nechushtai, R. A point mutation in the [2Fe-2S] cluster binding region of the NAF-1 protein (H114C) dramatically hinders the cluster donor properties. *Acta Crystallogr D Biol Crystallogr.* **2014,** *70 (pt 6)*, 1572-1578.

63. Wiley, S. E.; Paddock, M. L.; Abresch, E. C.; Gross, L.; van der Geer, P.; Nechushtai, R.; Murphy, A. N.; Jennings, P. A.; Dixon, J. E. The outer mitochondrial membrane protein mitoNEET contains a novel redox-active 2Fe-2S cluster. *J Biol Chem.* **2007,** *282 (33)*, 23745-23749.

64. Thermo Scientific Pierce Cell Lysis Technical Handbook. http://tools.thermofisher.com/content/sfs/brochures/1601757-Cell-Lysis-Handbook.pdf (accessed May 3, 2019).

65. Yang, J.; Ding, H. A Proposed DNA Binding Activity of Mitochondrial Iron-sulfur Protein Miner2. *Free Radical Biology and Medicine.* ***2017,*** *112 (1)*, 81.

66. Iosub-Amir, A.; Bai, F.; Sohn, Y.-S.; Song, L.; Tamir, S.; Marjault, H.-B.; Mayer, G.; Karmi, O.; Jennings, P. A.; Mittler, R.; Onuchic, J. N.; Friedler, A.; Nechushtai, R. The anti-apoptotic proteins NAF-1 and iASPP interact to drive apoptosis in cancer cells. *Chem Sci.* **2018,** *10 (3)*, 665-673.

67. Landry, A. P.; Ding, H. Redox control of human mitochondrial outer membrane protein MitoNEET [2Fe-2S] clusters by biological thiols and hydrogen peroxide. *J Biol Chem.* **2014,** *289 (7)*, 4307-4315.

68. Boyle, A. L. Applications of de novo designed peptides. *Peptide Applications in Biomedicine, Biotechnology and Bioengineering*. **2018,** 51-86.

69. Nechushtai, R.; Conlan, A. R.; Harir, Y.; Song, L.; Yogev, O.; Eisenberg-Domovich, Y.; Livnah, O.; Michaeli, D.; Rosen, R.; Ma, V.; Luo, Y.; Zuris, J. A.; Paddock, M. L.; Cabantchik, Z. I.; Jennings, P. A.; Mittler, R. Characterization of Arabidopsis NEET reveals an ancient role for NEET proteins in iron metabolism. *Plant Cell.* **2012,** *24 (5)*, 2139-2154.

70. Anthis, N. J.; Clore, G. M. Sequence-specific determination of protein and peptide concentrations by absorbance at 205 nm. *Protein Sci.* **2013,** *22 (6)*, 851-858.

71. Idiris, A.; Alam, M. T.; Ikai, A. Spring mechanics of alpha-helical polypeptide. *Protein Eng.* **2000,** *13 (11)*, 763-770.

72. Sheftel, A. D.; Stehling, O.; Pierik, A. J.; Elsässer, H.-P.; Mühlenhoff, U.; Webert, H.; Hobler, A.; Hannemann, F.; Bernhardt, R.; Lill, R. Humans possess two mitochondrial ferredoxins, Fdx1 and Fdx2, with distinct roles in steroidogenesis, heme, and Fe/S cluster biosynthesis. *Proc Natl Acad Sci U S A.* **2010,** *107 (26)*, 11775-11780.

73. Zuris, J. A.; Harir, Y.; Conlan, A. R.; Shvartsman, M.; Michaeli, D.; Tamir, S.; Paddock, M. L.; Onuchic, J. N.; Mittler, R.; Cabantchik, Z. I.; Jennings, P. A.; Nechushtai, R. Facile transfer of [2Fe-2S] clusters from the diabetes drug target mitoNEET to an apo-acceptor protein. *Proc Natl Acad Sci U S A.* **2011,** *108 (32)*, 13047-13052.

74. Bak, D. W.; Zuris, J. A.; Paddock, M. L.; Jennings, P. A.; Elliott, S. J. Redox characterization of the FeS protein MitoNEET and impact of thiazolidinedione drug binding. *Biochemistry.* **2009,** *48 (43)*, 10193-10195.

75. Dicus, M. M.; Conlan, A.; Nechushtai, R.; Jennings, P. A.; Paddock, M. L.; Britt, R. D.; Stoll, S. Binding of histidine in the (Cys)3(His)1-coordinated [2Fe-2S] cluster of human mitoNEET. *J Am Chem Soc.* **2010,** *132 (6)*, 2037-2049.

76. Hagen, W. R. EPR spectroscopy of complex biological iron-sulfur systems. *J Biol Inorg Chem.* **2018,** *23 (4)*, 623-634.

77. Zuris, J. A.; Halim, D. A.; Conlan, A. R.; Abresch, E. C.; Nechushtai, R.; Paddock, M. L.; Jennings, P. A. Engineering the redox potential over a wide range within a new class of FeS proteins. *J Am Chem Soc.* **2010,** *132 (38)*, 13120-13122.

78. Stevens, R.; Stevens, L.; Price, N. C. The stabilities of various thiol compounds used in protein purifications. *Biochemical Education.* **1983,** *11 (2)*, 70.

79. Li, X.; Wang, Y.; Tan, G.; Lyu, J.; Ding, H. Electron transfer kinetics of the mitochondrial outer membrane protein mitoNEET. *Free Radic Biol Med.* **2018,** *121*, 98-104.

80. Landry, A. P.; Cheng, Z.; Ding, H. Reduction of mitochondrial protein mitoNEET [2Fe-2S] clusters by human glutathione reductase. *Free Radic Biol Med.* **2015,** *81*, 119-127.

81. Hoshi, T.; Heinemann, S. Regulation of cell function by methionine oxidation and reduction. *J Physiol.* **2001,** *531 (pt 1)*, 1-11.

82. Seo, A.; Jackson, J. L.; Schuster, J. V.; Vardar-Ulu, D. Using UV-absorbance of intrinsic dithiothreitol (DTT) during RP-HPLC as a measure of experimental redox potential in vitro. *Anal Bioanal Chem.* **2013,** *405 (19)*, 6379-6384.

83. Cleland, W. W. DITHIOTHREITOL, A NEW PROTECTIVE REAGENT FOR SH GROUPS. *Biochemistry.* **1964,** *3*, 480-482.

84. Hosseinzadeh, P.; Lu, Y. Design and fine-tuning redox potentials of metalloproteins involved in electron transfer in bioenergetics. *BBA-Bioenergetics.* **2016,** *1857 (5)*, 557-581.

85. Wallrapp, F. H.; Voityuk, A. A.; Guallar, V. In-silico assessment of protein-protein electron transfer. a case study: cytochrome c peroxidase--cytochrome c. *PLoS Comput Biol.* **2013,** *9 (3)*, e1002990.

86. Holder, P. G.; Pizano, A. A.; Anderson, B. L.; Stubbe, J.; Nocera, D. G. Deciphering radical transport in the large subunit of class I ribonucleotide reductase. *J Am Chem Soc.* **2012,** *134 (2)*, 1172-1180.

87. Winkler, J. R.; Gray, H. B. Could tyrosine and tryptophan serve multiple roles in biological redox processes? *Philos Trans A Math Phys Eng Sci.* **2015,** *373 (2037)*, pii: 20140178.

88. Butchosa, C.; Simon, S.; Voityuk, A. A. Electron transfer from aromatic amino acids to guanine and adenine radical cations in pi stacked and T-shaped complexes. *Org Biomol Chem.* **2010,** *8 (8)*, 1870-1875.

89. Larson, B. C.; Pomponio, J. R.; Shafaat, H. S.; Kim, R. H.; Leigh, B. S.; Tauber, M. J.; Kim, J. E. Photogeneration and Quenching of Tryptophan Radical in Azurin. *J Phys Chem B.* **2015,** *119 (29)*, 9438-9449.

90. Stuchebrukhov, A. A. Long-Distance Electron Tunneling in Proteins: A New Challenge for Time-Resolved Spectroscopy. *Laser Phys.* **2010,** *20 (1)*, 125-138.